

中国激光

基于氧化镓日盲紫外光电探测器的研究进展

王江, 罗林保*

合肥工业大学电子科学与应用物理学院, 安徽 合肥 230009

摘要 日盲紫外探测器以其较高的探测灵敏度和较低的背景噪声广泛应用于导弹制导、空间安全通信、臭氧层空洞监测和火焰检测等军事和民用领域。氧化镓(Ga_2O_3)是一种典型的超宽禁带半导体材料, 其较大的禁带宽度(4.2~5.3 eV)几乎占据太阳光谱的整个日盲波段, 被认为是制备日盲紫外探测器的理想材料。主要介绍了 Ga_2O_3 的不同晶体结构和基本特性, 并综述了基于多种 Ga_2O_3 结构的日盲紫外探测器的研究进展。基于 Ga_2O_3 纳米线的器件的最大光响应度 $R > 10^3 \text{ A/W}$, 外量子效率能达到10% ; Ga_2O_3 单晶器件的光响应度高达 $10^3 \sim 10^5 \text{ A/W}$, 外量子效率超过10%, 响应速度较快(μs级)。 Ga_2O_3 基异质结、p-n结和肖特基结的日盲探测器表现出的自驱动特性使其在无需外加电源条件下就能正常工作, 这在特殊环境下具有较大的应用潜力。

关键词 光电探测器; 氧化镓; 超宽禁带半导体; 日盲紫外; 光响应

中图分类号 TN23

文献标志码 A

doi: 10.3788/CJL202148.1100001

1 引言

太阳光入射到地球表面时, 波长范围为200~280 nm的深紫外(DUV)光在大气臭氧层的强烈吸收导致地球表面几乎不存在该波段的紫外光, 因而将该波段定义为日盲区。针对该波段进行检测的日盲紫外探测器由于具有背景噪声低、灵敏度高、抗干扰性强等特点, 在太阳紫外线检测、天文学、空间安全通信和光学成像等领域具有十分重要的应用前景^[1-6]。目前, 由于硅工艺高度成熟且成本较低, 主要商用日盲紫外光电探测器件均由硅材料制成。但硅材料较窄的禁带宽度(1.1~1.3 eV)使得硅基光电探测器在用于检测日盲波段时通常需要添加光学滤光片且探测效率偏低, 这限制了其在日盲探测领域的应用^[1,7-9]。近年来, 飞速发展的半导体技术和器件制备工艺激起了人们对基于宽禁带半导体材料的日盲紫外探测器的浓厚研究兴趣, 同时, 宽带隙半导体较高的热稳定性和化学稳定性使其可应用于恶劣环境中^[10]。在众多 $\text{Al}_x\text{Ga}_{1-x}\text{N}$ 和 $\text{Mg}_x\text{Zn}_{1-x}\text{O}$ 基日盲紫外探测器研究报道中, 对材料的带隙调控

分别通过调节Al和Mg含量实现。由于Al原子较大的附着系数和较低的表面迁移速率, Al含量较高时会导致 $\text{Al}_x\text{Ga}_{1-x}\text{N}$ 外延层位错密度较高^[11-13], 而Mg含量过高时 $\text{Mg}_x\text{Zn}_{1-x}\text{O}$ 会出现相分离, 这些因素会导致器件性能偏低^[14-15]。

氧化镓(Ga_2O_3)作为一种典型超宽禁带半导体材料, 具有较高的热稳定性、化学稳定性和平均透过率等特点^[16-18]。 Ga_2O_3 优异的物理化学性能使其在电力电子器件和日盲紫外探测器方面具有广泛的应用前景, 同时, Ga_2O_3 晶体生长技术方面的突破性进展极大地推动了 Ga_2O_3 薄膜外延、日盲紫外探测、电力电子等器件的研究。此外, Ga_2O_3 在2018年被列入我国重点研发计划“战略性先进电子材料”重点专项“超宽禁带半导体材料与器件研究(基础研究类)”, 这也极大带动了国内科研人员对 Ga_2O_3 材料深入研究的积极性。

本文首先介绍了 Ga_2O_3 材料的物理化学特性, 并进一步综述了基于不同结构 Ga_2O_3 的日盲紫外探测器的研究进展, 这对 Ga_2O_3 在日盲紫外探测方面的进一步广泛应用具有一定指导意义。

收稿日期: 2020-09-16; 修回日期: 2020-11-06; 录用日期: 2020-12-28

基金项目: 国家自然科学基金(62074048)、中央高校基础研究基金(JZ2018HGXC0001)、安徽省先进功能材料和器件重点实验室开放基金(4500-411104/011)

*E-mail: luolb@hfut.edu.cn

2 Ga_2O_3 的基本特性

众所周知, Ga_2O_3 作为一种典型的超宽禁带半导体, 近年来得到了国内外研究人员的广泛关注。1952年, Roy等^[19]报道了 $\text{Al}_2\text{O}_3\text{-}\text{Ga}_2\text{O}_3\text{-H}_2\text{O}$ 相平衡系统及不同形态结构的 Ga_2O_3 (标记为 α , β , γ , δ 和 ϵ), 同时研究发现5种结构的 Ga_2O_3 在不同条件下可以相互转化。表1列出了 Ga_2O_3 不同相的基本参数, $\alpha\text{-}\text{Ga}_2\text{O}_3$ 为刚玉结构, 属于 $\bar{\text{R}3c}$ 空间群^[20], 晶格常数 $a=b=4.98\times10^{-10}\text{ m}$, $c=13.40\times10^{-10}\text{ m}$ ^[21], 禁带宽度约为5.3 eV^[22], $\alpha\text{-}\text{Ga}_2\text{O}_3$ 较大的禁带宽度使其可应用于制备日盲紫外探测器, 此外, 可以通过掺杂对 $\alpha\text{-}\text{Ga}_2\text{O}_3$ 的电子导电性进行有效调控(如Sn, F和Si掺杂)^[23-25]。同时, $\alpha\text{-}\text{Ga}_2\text{O}_3$ 可以与其他刚玉结构的氧化物材料(Al_2O_3 , Fe_2O_3 , Cr_2O_3)形成

固溶体, 从而可用于制备新型功能材料^[26-28]。 $\gamma\text{-}\text{Ga}_2\text{O}_3$ 与 $\gamma\text{-}\text{Al}_2\text{O}_3$ 类似, 均属于立方晶系, $\bar{\text{Fd}3m}$ 空间群^[29-30], 值得注意的是, $\gamma\text{-}\text{Ga}_2\text{O}_3$ 与 $\gamma\text{-}\text{Al}_2\text{O}_3$ 的固溶体近年来被应用于去除废气中氮氧化物^[31-33]。 $\epsilon\text{-}\text{Ga}_2\text{O}_3$ 属于六角晶系, $\text{P}63\text{mc}$ 空间群^[34-36], 类似于六角晶系的 GaN 和 ZnO , 在 SiC , AlN , MgO 和 Al_2O_3 等衬底上可以异质外延生长高质量的 $\epsilon\text{-}\text{Ga}_2\text{O}_3$ 薄膜^[37-40], 这表明 $\epsilon\text{-}\text{Ga}_2\text{O}_3$ 在光电子器件领域具有较大的应用潜力。 $\delta\text{-}\text{Ga}_2\text{O}_3$ 为立方晶系, $\bar{\text{Ia}3}$ 空间群^[41], 与 In_2O_3 和 Mn_2O_3 结构类似^[29]。然而, 在5种同分异构体中, 常温常压下 $\beta\text{-}\text{Ga}_2\text{O}_3$ 的物理化学特性最稳定, 其他结构均为亚稳态, 目前报道的大多数日盲紫外探测器和电力电子器件都是基于 $\beta\text{-}\text{Ga}_2\text{O}_3$, 因此以下部分主要讨论 $\beta\text{-}\text{Ga}_2\text{O}_3$ 的性质及其在日盲紫外探测器中的应用。

表1 Ga_2O_3 多晶的基本参数总结^[15,42]

Table 1 Summary of basic parameters of Ga_2O_3 polycrystalline^[15,42]

Polymorph	Lattice constant / (10^{-10} m)	Bandgap /eV	Structure	Space group	Optical dielectric constant
α	$a,b=4.98\text{-}5.04$, $c=13.4\text{-}13.60$	5.3	Rhombohedral	$\bar{\text{R}3c}$	3.03-3.80
β	$a=12.12\text{-}12.34$, $b=3.03\text{-}3.04$, $c=5.80\text{-}5.87$	4.2-4.9	Monoclinic	$\text{C}2/\text{m}$	2.82-3.57
γ	$a=8.24\text{-}8.30$	5.0	Cubic	$\bar{\text{Fd}3m}$	-
δ	$a=9.40\text{-}10.0$		Cubic	$\bar{\text{Ia}3}$	-
ϵ	$a=5.06\text{-}5.12$, $b=8.69\text{-}8.79$, $c=9.30\text{-}9.40$	4.9	Hexagonal	$\text{P}63\text{mc}$	-

$\beta\text{-}\text{Ga}_2\text{O}_3$ 属于单斜系, $\text{C}2/\text{m}$ 空间群, 晶格常数 $a=12.23\times10^{-10}\text{ m}$, $b=3.04\times10^{-10}\text{ m}$, $c=5.80\times10^{-10}\text{ m}$, $\alpha=\gamma=90^\circ$, $\beta=103.7^\circ$ ^[43-45]。图1为 $\beta\text{-}\text{Ga}_2\text{O}_3$ 的晶体结构模型图, 可以看到 $\beta\text{-}\text{Ga}_2\text{O}_3$ 晶体学晶胞具有两个不同位置的 Ga 和三个不同位置的 O。一部分 Ga 原子位于 Ga(I) 位置, 与周围 4 个 O 形成略微扭曲的四面体结构; 另一部分 Ga 在 Ga(II) 位置, 与 6 个 O 离子形成高度扭曲的八面体结构。每个 O(I) 具有三重配位, 并且位于两个八面体和一个四面体的交点处。每个 O(II) 也具有三重配位, 由一个八面体和两个四面体共享。每个 O(III) 具有四重配位, 位于三个八面体和一个四面体的角上^[45-47]。

表2列出了 $\beta\text{-}\text{Ga}_2\text{O}_3$ 与目前常用半导体材料的基本物理特性, 从表中数据可以看出, 与其他半导

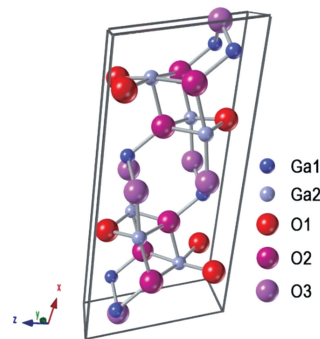


图1 $\beta\text{-}\text{Ga}_2\text{O}_3$ 的晶体结构^[45]

Fig. 1 Crystal structure of $\beta\text{-}\text{Ga}_2\text{O}_3$ ^[45]

体材料相比, $\beta\text{-}\text{Ga}_2\text{O}_3$ 具有较大的禁带宽度(4.2~4.9 eV), 较大的击穿电场(8 MV/cm)(约为 GaN 的两倍), 介电常数 ϵ 为 10。由于 $\beta\text{-}\text{Ga}_2\text{O}_3$ 带隙较大, 因此室温下无缺陷态的 $\beta\text{-}\text{Ga}_2\text{O}_3$ 材料呈绝缘

态,但实际材料制备过程中难免会引入氧空位(V_O)、镓空位(V_{Ga})和镓间隙(Ga_i)等缺陷态,这会使得制备的 $\beta\text{-Ga}_2\text{O}_3$ 偏离理想化学计量比,因此实际生长的 $\beta\text{-Ga}_2\text{O}_3$ 通常表现出n型导电特性^[48-49]。 $\beta\text{-Ga}_2\text{O}_3$ 的固有导电性源自晶体中形成的点缺陷所导致的自由电子。大多数研究表明, V_O 是影响 $\beta\text{-Ga}_2\text{O}_3$ 导电性的主要缺陷^[50-51]。近年来,人们通过

掺杂Si和Sn等四价元素作为浅施主杂质以调节 $\beta\text{-Ga}_2\text{O}_3$ 的导电性。随着掺杂浓度的变化,n型 $\beta\text{-Ga}_2\text{O}_3$ 的电阻率在 $10^{-3}\sim10^{12}\Omega\cdot\text{cm}$ 的范围内变化,迁移率可达到 $180\text{ cm}^2/(\text{V}\cdot\text{s})$ [实验估算值可达 $300\text{ cm}^2/(\text{V}\cdot\text{s})$]^[52-54]。 $\beta\text{-Ga}_2\text{O}_3$ 优越的光学及电学特性使其在日盲紫外探测、透明电极、高功率半导体器件和气体传感等方面具有很好的应用前景。

表2 $\beta\text{-Ga}_2\text{O}_3$ 与其他常用半导体的基本特性^[55]Table 2 Properties of $\beta\text{-Ga}_2\text{O}_3$ and other more commonly used semiconductors^[55]

Parameter	Si	GaAs	GaN	4H-SiC	MgZnO	Diamond	$\beta\text{-Ga}_2\text{O}_3$
Bandgap E_g / eV	1.10	1.43	3.40	3.25	3.70~7.80	5.50	4.20~4.90
Relative dielectric constant ϵ	11.8	12.9	9.0	9.7	4.6	5.50	10.0
Breakdown field / ($\text{MV}\cdot\text{cm}^{-1}$)	0.3	0.4	3.3	2.5	—	10.0	8.0
Electron mobility / ($\text{cm}^2\cdot\text{V}^{-1}\cdot\text{s}^{-1}$)	1480	8400	1250	1000	250	2000	300
Thermal conductivity / ($\text{W}\cdot\text{cm}^{-1}\cdot\text{K}$)	1.5	0.5	2.3	4.9	1.2	20.0	0.1~0.3
Saturation velocity ($10^7\text{ cm}\cdot\text{s}^{-1}$)	1	1.2	2.5	2	—	1	1.8~2
Baliga ($\epsilon\cdot\mu\cdot E_c^3$)	1	14.7	846	317	—	24660	3444
Keyes [$\lambda/(4\pi\epsilon)$] ^{1/2}	1	0.3	1.8	3.6	—	41.5	0.2

3 Ga_2O_3 材料的生长合成

高质量的材料是制备高性能光电器件的基础保障。近年来,国内外研究者们通过不同方法制备高质量 Ga_2O_3 材料,并将其用于电力电子器件及光电子器件。由于 Ga_2O_3 为n型导电材料且带隙较大,在 Ga_2O_3 制备过程中,人们采用Si、Ge和Sn等作为掺杂剂,通过分子束外延(MBE)和金属有机化学气相沉积(MOCVD)等方法外延薄膜,实现了载流子的有效调控^[56-58]。此外,p型 Ga_2O_3 在制备器件中仍然至关重要,但实现高质量的p型 Ga_2O_3 仍是一项重要挑战。近年来,人们通过多种方法对 Ga_2O_3 p型导电机制进行了广泛研究。基于Mg掺杂p型GaN的成功经验,研究人员尝试通过Mg掺杂实现 Ga_2O_3 p型导电,但实验发现Mg掺杂 Ga_2O_3 的受主能级较深^[59],且薄膜电阻较大^[60]。虽然Zn掺杂 Ga_2O_3 具有较浅的受主能级(电离能为 $0.25\sim0.5\text{ eV}$),但薄膜电阻率仍然较高^[61-62]。而N掺杂可以形成与 Ga_2O_3 本征缺陷相关的复合体缺陷,这些缺陷会补偿p型导电^[63]。迄今为止,高质量稳定的p型 Ga_2O_3 仍然难以实现。

3.1 纳米结构

目前,研究人员合成 $\beta\text{-Ga}_2\text{O}_3$ 纳米材料的方法主要有化学气相沉积(CVD)^[4,64]、溶液法^[65-66]、气-

液-固法^[67-70]、气相传输^[71]等。此外,由于 $\beta\text{-Ga}_2\text{O}_3$ 晶体具有独特的两个解理面(100)和(001),因此人们还可通过机械剥离法从 $\beta\text{-Ga}_2\text{O}_3$ 晶体上获得高质量的 $\beta\text{-Ga}_2\text{O}_3$ 准二维纳米薄片^[72-77]。过去十余年来,人们对不同形态的 $\beta\text{-Ga}_2\text{O}_3$ 纳米材料的基本物理特性进行了广泛研究,并将这类材料用于各种电子或光电子器件。

3.2 单晶

在 Ga_2O_3 的多种结构中, β 相 Ga_2O_3 具有优异的物理特性且熔点高达 $1740\text{ }^\circ\text{C}$,经过长期研究,人们已提出焰熔法^[78-79]、浮区(FZ)法^[80-81]、垂直布里奇曼(VB)法^[82-83]、导模(EFG)法^[84-85]、提拉(CZ)法^[86-87]等方法生长高质量的 $\beta\text{-Ga}_2\text{O}_3$ 单晶衬底,这为实现基于 $\beta\text{-Ga}_2\text{O}_3$ 单晶的高性能器件创造了有利条件。1964年,Chase^[88]通过焰熔法首次成功制备出直径约为 1 cm 的 $\beta\text{-Ga}_2\text{O}_3$ 单晶,但其晶体尺寸较小,结晶质量不高。过去十余年里,随着单晶生长技术的不断发展,人们生长的 $\beta\text{-Ga}_2\text{O}_3$ 单晶质量不断提高。2004年,日本首次报道了通过浮区法生长的 1 inch ($1\text{ inch}=2.54\text{ cm}$) $\beta\text{-Ga}_2\text{O}_3$ 晶体,实现了(100)、(010)和(001)方向晶片的抛光切割,样品X射线衍射(XRD)半峰全宽约为 0.09° ,载流子浓度约为 10^{17} cm^{-3} ^[89]。此外,有研究发现在 $\beta\text{-Ga}_2\text{O}_3$ 单晶生长过程中通入的 CO_2 在高温下能提供生长

所需的高氧分压,在未掺杂条件下,晶体的颜色、光学及电学特性与生长条件(气氛、压力和温度梯度)密切相关, $\beta\text{-Ga}_2\text{O}_3$ 晶体的电阻率约为 $0.1 \Omega \cdot \text{cm}$,迁移率约为 $120 \text{ cm}^2/(\text{V} \cdot \text{s})$,载流子浓度约为 10^{17} cm^{-3} ,而 Sn 掺杂可以将载流子浓度有效调控至 10^{19} cm^{-3} ^[86,90]。由于晶体生长过程中残留的 Si 杂质,非故意掺杂 $\beta\text{-Ga}_2\text{O}_3$ 晶体的有效施主浓度($N_d - N_a$)受 Si 含量控制,但 Si 浓度较高时,晶体出现裂纹^[91]。近年来,国内对于 $\beta\text{-Ga}_2\text{O}_3$ 单晶生长的研究成果显著;2006 年,中国科学院上海光学精密机械研究所采用浮区法生长 $\beta\text{-Ga}_2\text{O}_3$ 单晶,这是国内首次报道 Ga_2O_3 单晶生长^[81]。2017 年,山东大学通过导模法生长出 1 inch $\beta\text{-Ga}_2\text{O}_3$ 单晶^[85]。同年,同济大学与中国科学院上海硅酸盐研究所采用导模法成功制备出了 2 inch $\beta\text{-Ga}_2\text{O}_3$ 单晶^[92]。2018 年,中国电子科技集团公司第 46 研究所利用导模法生长出 2 inch $\beta\text{-Ga}_2\text{O}_3$ 单晶^[93]。 $\beta\text{-Ga}_2\text{O}_3$ 单晶材料的成功制备为研制具有较低暗电流、较高探测灵敏度的 $\beta\text{-Ga}_2\text{O}_3$ 单晶日盲紫外探测器奠定了基础。

3.3 薄膜

通常情况下,薄膜材料的制备较为灵活且制备工艺的可重复性较高,因此沉积高质量的 $\beta\text{-Ga}_2\text{O}_3$ 薄膜有利于实现高性能的 $\beta\text{-Ga}_2\text{O}_3$ 器件。近年来,人们尝试采用分子束外延(MBE)^[5,94-99]、金属有机化学气相沉积(MOCVD)^[100-105]、脉冲激光沉积(PLD)^[57,106-109]、原子层沉积(ALD)^[110-112]、溶胶-凝胶法(sol-gel)^[113-117]、射频磁控溅射(RFMS)^[118-124] 和卤化物气相外延(HVPE)^[125-130] 等方法生长 $\beta\text{-Ga}_2\text{O}_3$ 薄膜。本节将结合国内外研究现状,主要介绍 $\beta\text{-Ga}_2\text{O}_3$ 薄膜外延生长的研究进展及当前所面临的主要技术挑战。

高压 $\beta\text{-Ga}_2\text{O}_3$ 器件通常需要薄膜外延层较厚且掺杂浓度较低,而 MBE 能较好地用于 $\beta\text{-Ga}_2\text{O}_3$ 薄膜同质外延,从而可用于生长高压器件的外延层。研究表明当外延晶面从(100)变为(010)面时,薄膜生长速率增加了 10 倍以上,且厚度达 $0.7 \mu\text{m}$ 时薄膜表面仍然较光滑[均方根(RMS)粗糙度为 0.7 nm]。此外,通过改变 Sn 掺杂浓度,外延薄膜载流子浓度可达 $10^{16} \sim 10^{19} \text{ cm}^{-3}$,使用 Ge 代替 Sn 掺杂时,薄膜电子迁移率得到明显改善^[56,131]。采用 MBE 生长 Si 掺杂 $\beta\text{-Ga}_2\text{O}_3$ 薄膜时,产生的挥发性 SiO 会导致 Si 流量出现异常,而活性氧含量能有效抑制 SiO 产生^[99]。研究发现,MOCVD 外延生长的 $\beta\text{-Ga}_2\text{O}_3$ 薄膜在室温下

的迁移率较高^[132-133];而随着 Si 掺杂浓度的升高,薄膜电子迁移率从 $120 \text{ cm}^2 \cdot \text{V}^{-1} \cdot \text{s}^{-1}$ 降到 $13 \text{ cm}^2 \cdot \text{V}^{-1} \cdot \text{s}^{-1}$,自由载流子浓度从 $1.6 \times 10^{17} \text{ cm}^{-3}$ 增加到 $8.0 \times 10^{19} \text{ cm}^{-3}$,生长速率达到 $4 \mu\text{m}/\text{h}$ ^[134]。相比之下,通过 PLD 同质外延的 $\beta\text{-Ga}_2\text{O}_3$ 薄膜具有较高的载流子浓度($8.0 \times 10^{19} \text{ cm}^{-3}$)和电导率(732 S/m),这能较好地用于 $\beta\text{-Ga}_2\text{O}_3$ 器件的低电阻欧姆接触层^[57]。结合众多研究报道发现,人们通过多种方法生长的 $\beta\text{-Ga}_2\text{O}_3$ 薄膜已经能较好地应用于透明电极和日盲紫外探测器领域,而对于功率器件,薄膜性能还需进一步提升。

4 Ga_2O_3 日盲紫外探测器的主要结构类型及技术进展

不同结构的 Ga_2O_3 日盲紫外探测器不仅在制备成本及应用环境方面有显著区别,对应的器件性能也存在较大差异,目前基于 Ga_2O_3 日盲探测器的典型结构包括以下几种。

1) 光电导型器件。该类器件主要依赖半导体的光敏特性,即光电导体的电导率随光照条件发生明显变化。在所有类型的探测器中,光电导探测器以其便利性得到了最广泛的研究。但制备用于光电导型器件的半导体材料时往往引入缺陷态,因此光电导探测器在实际应用中存在持续光电导效应,器件衰减时间普遍较长,暗电流较大,同时信噪比较低。

2) 肖特基结型器件。肖特基结型光电探测器主要基于金属和半导体材料在界面处形成的肖特基势垒。根据 Schotthy-Mott 模型,器件的整流特性是由金属和半导体之间的势垒引起,该类器件是一种多子器件。在光照下,耗尽区产生的电子-空穴对被迅速收集到电极,因此器件响应速度较快。同时由于肖特基势垒的存在,器件在暗环境下的暗电流较低,器件的响应度(R)和信噪比较高。

3) 金属-半导体-金属结构(MSM)型器件。MSM 型光电探测器是基于肖特基结的一种简易结构,主要由金属和半导体接触形成的两个背靠背肖特基势垒构成。该类器件的电极的宽度和间距对器件性能影响较大,器件具有较大增益。MSM 型光电探测器通常结构简单,单位面积内结电容较小,易于集成且与晶体管工艺兼容,但金属电极使得器件有效光吸收面积较小,因此,这种结构器件的响应度低。

4) p-n 结和异质结型器件。与肖特基结不同的是,p-n 结主要由两种不同导电类型的半导体构成,

其原理是光生伏特效应。在光照条件下,光生电子-空穴对在内建电场作用下向相反方向移动,形成光电流。由于 p-n 结为少子器件,因此光伏效应产生的光生少数载流子对器件的影响较大,通常器件灵敏度高。由于 p-n 结势垒的存在,器件具有二极管整流特性。

与 p-n 结类似,异质结由两种不同的半导体材料构成。由于构建异质结的两种材料内部载流子浓度和费米能级不同,在接触后载流子的扩散会使费米能级持平,而这种扩散同样会在异质结界面处形成内建电场。异质结制备简单,无需考虑与材料导电类型相关的掺杂问题。异质结和 p-n 结型日盲探测器在自驱动器件方面具有较大应用潜力。

过去十余年里,人们不断优化 Ga_2O_3 日盲紫外探测器的器件结构以改善其探测性能。MSM 结构由于制备工艺简便而被广泛应用,目前 MSM 型 Ga_2O_3 日盲紫外探测器表现出较低的暗电流 (pA 量级) 及较大的光暗电流比 ($>10^5$)^[73,135-136], 同时该器件结构也能较好地应用于 Ga_2O_3 探测器阵列及柔性器件^[137-141]。在最近的研究中, Ga_2O_3 肖特基结型日盲探测器往往表现出超高的整流比 ($>10^6$)^[142-143]、较高的响应度 ($>10^3 \text{ A/W}$)^[144] 及较短的响应时间 (μs 量级)^[145]。由于 Ga_2O_3 的 n 型导电特性,近年来研究人员结合其他 p 型 (NiO,

GaN, diamond, SiC 等)^[146-149] 或 n 型 ($\text{ZnO}, \text{SrTiO}_3, \text{MoS}_2$ 等)^[121,150-151] 材料制备 p-n 结或异质结日盲探测器,其响应时间明显缩短,且器件通常具有自驱动特性。例如, $\text{ZnO}-\text{Ga}_2\text{O}_3$ 核-壳异质结日盲探测器的响应度高达 10^3 A/W , 相应的探测度高达 10^4 Jones , 响应时间达 μs 量级^[150]。

5 Ga_2O_3 基日盲紫外探测器的研究进展

5.1 Ga_2O_3 纳米结构日盲紫外探测器

目前,国内外研究者们已将不同形态结构的 Ga_2O_3 纳米材料(纳米线、纳米片和纳米柱等)应用于日盲紫外探测器,而纳米材料较高的表面体积比使得器件具有较高的探测灵敏度。2006 年, Feng 等^[152]通过在可控环境中直接蒸发 Ga 生长 β - Ga_2O_3 纳米线。制备的纳米线直径大多为几十纳米,长度达数十微米[图 2(a)]。随后采用光刻技术及电子束蒸发沉积两个 Au 电极,结合单根纳米线制备日盲紫外探测器,图 2(a)中插图给出了器件的扫描电子显微镜(SEM)图像。如图 2(b)所示,器件暗电流达 pA 量级。在一 8 V 偏压、254 nm 光照下,器件光电流迅速增加至 nA 级别[图 2(c)],具有明显的日盲光响应,同时器件具有较短的上升/下降时间 (0.45/0.09 s)[图 2(d)]。

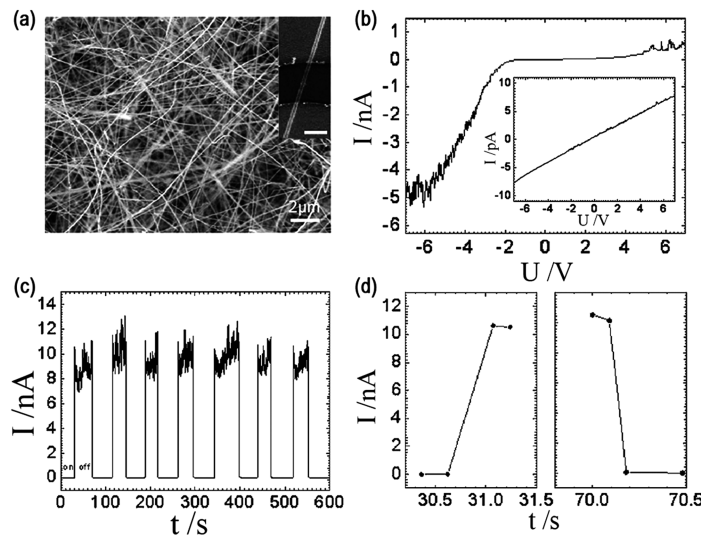


图 2 β - Ga_2O_3 纳米线的形貌及器件的光电响应^[152]。(a) 镀金衬底上生长的 β - Ga_2O_3 纳米线 SEM 图像;(b) 器件在 254 nm 光照和暗环境(插图)的 I - V 曲线;(c) 器件对 254 nm 光照的时间响应曲线;(d) 首次光“开”和“关”上升沿和下降沿的放大图

Fig. 2 Morphology of β - Ga_2O_3 nanowires and photoelectric response of device^[152]. (a) SEM image of the β - Ga_2O_3 nanowires grown on the Au-coated silicon substrate; (b) I - V curves of the detector under 254 nm light illumination and dark condition (inset); (c) time response of the device to light at 254 nm; (d) enlargement of the rising and falling edges for the light “on” and “off” for the first time

2010 年, Li 等^[4]通过 CVD 方法在不同温度下合成 $\beta\text{-Ga}_2\text{O}_3$ 纳米线, 纳米线直径约为 60 nm, 且室温光致发光(PL)谱显示出较强的紫外线 C(UVC)发射, 这也是首次报道 $\beta\text{-Ga}_2\text{O}_3$ 的本征 PL 发射。此外, 紫外线 A(UVA)到可见光区域出现多个发射峰, 这些缺陷发射峰可能是由施主缺陷(V_O)与受主缺陷(V_{Ga} 、 $V_{Ga}-V_O$)的复合引起。通过桥接 $\beta\text{-Ga}_2\text{O}_3$ 纳米线制备桥式结构日盲探测器, 该器件与传统纳米器件相比具有制备工艺简单高效、成本低的特点; 由于电极与桥接纳米线为同种材料, 因此不存在接触势垒。器件具有较高的 250 nm/280 nm 抑制比($\sim 2 \times 10^3$), 同时对波长大于 280 nm 的光照几乎无响应且器件响应时间较短(20 ms)。

2014 年, Zou 等^[153]合成(100)面向 $\beta\text{-Ga}_2\text{O}_3$ 纳米带并制备了在常温和高温下均具有高光电性能的 $\beta\text{-Ga}_2\text{O}_3$ 纳米带日盲紫外探测器。合成的纳米带长度达几十到几百微米, 而一个单独的 $\beta\text{-Ga}_2\text{O}_3$ 纳米带“单元”是由几个平行且重叠的纳米带形成的多层结构。此外, $\beta\text{-Ga}_2\text{O}_3$ 纳米带经过弯折后仍能完全恢复, 而将纳米带从 100 °C 加热到 1000 °C 时, 形貌未发生变化。采用两个 Au 电极和纳米带制备日盲探测器, 器件的最大光响应度位于 250 nm。器件暗电流小于 10^{-13} A, 具有较高的信噪比。在“开”、“关”光循环条件下, 器件表现出较高的可重复性和稳定性, 同时, $\beta\text{-Ga}_2\text{O}_3$ 纳米带器件的响应度和外量子效率(EQE)较高, 分别为 850 A/W 和 $4.2 \times$

$10^3\%$ [内量子效率(IQE)是评估 LED 及太阳能电池的一项重要参数指标, 其影响因素较多, 因此较少被用来评估光电探测器, 为方便起见, 目前主要讨论光电探测器的外量子效率]。合成的多层结构 $\beta\text{-Ga}_2\text{O}_3$ 纳米带在光传输过程中由于反射和折射, 有效增大了光活性面积和光吸收, 从而使得光电流增加。值得一提的是, 器件在高温(328~433 K)条件下仍表现出较高的光电响应, 在 433 K 时, 器件对 250 nm 光照的 R 和 EQE 分别为 650 A/W 和 $3.2 \times 10^3\%$, 这比众多半导体器件在室温和高温环境下的性能都高。该工作制备的 $\beta\text{-Ga}_2\text{O}_3$ 纳米带日盲探测器在高温下的优越性对制备高性能光电开关和高温光电探测器具有重要的指导意义。

2019 年, Qiao 等^[135]采用 mist-CVD 生长 $\alpha\text{-Ga}_2\text{O}_3$ 并制备了 Al 纳米等离子体增强的 MSM 结构 $\alpha\text{-Ga}_2\text{O}_3$ 日盲紫外探测器, 图 3(a)中插图给出了器件结构示意图。当器件电极间距逐渐减小时, 光谱响应度逐渐增大, 且最大响应度为 3.36 A/W, 响应波长主要集中在日盲区[图 3(b)]。此外, 器件暗电流极低(1 pA), 光暗电流比较高(10^5), 器件的光电流同样随电极间距的减小而增大[图 3(c)]。同年, Wang 等^[154]在玻璃纤维织物衬底上原位合成 $\beta\text{-Ga}_2\text{O}_3$ 纳米线并制备了柔性日盲紫外探测器。基于纳米线制备的日盲探测器在 20 V 偏压下的暗电流为 8.4 nA, 在 254 nm 光照下, 光电流增加至 2.18 μ A, 光暗电流比为 260, 器件具有较好的日盲光电特性。

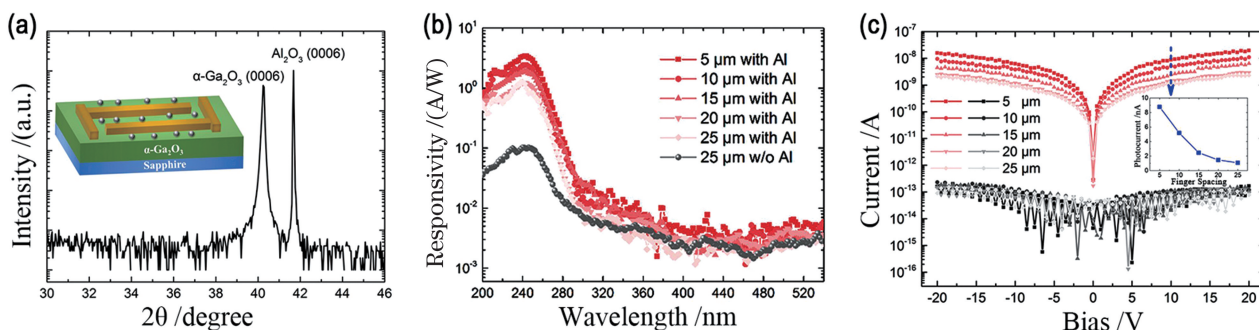


图 3 Ga_2O_3 的结构特性及其器件性能^[135]。(a)生长在蓝宝石衬底上的 $\alpha\text{-Ga}_2\text{O}_3$ XRD 谱, 插图为器件示意图;(b)器件在 5 V 偏压下的光谱响应;(c)器件在黑暗(黑线)及光照下的 $I\text{-}V$ 特性

Fig. 3 Structural characteristics of Ga_2O_3 and performance of the device^[135]。(a) X-ray diffraction (XRD) pattern of the $\alpha\text{-Ga}_2\text{O}_3$ grown on the sapphire substrate. The inset shows the schematic of the device structure; (b) spectral responsivity of the photodetectors at 5 V bias; (c) $I\text{-}V$ characteristics of the devices in the dark (black line) and under illumination

与传统红外成像技术相比, 日盲紫外成像技术具有背景干扰小、灵敏度高和分辨率高等特点, 这使得该技术能较好地应用于军事和民用领域。近年来, Ga_2O_3 在日盲成像方面的应用研究成效显著,

Ga_2O_3 基日盲成像器件的成像效果较明显。2019 年, 本课题组通过气-固合成技术生长 $\beta\text{-Ga}_2\text{O}_3$ 单晶纳米线, 生长温度在 1100 °C 时, 纳米线长度达几百微米, 直径在 100~500 nm 范围内; 将纳米线转移

至 SiO_2/Si 衬底上, 通过电子束蒸发镀 Au 电极制备日盲探测器^[155]。器件暗电流较低(80 pA)且表现出非线性行为, 这与 $\beta\text{-Ga}_2\text{O}_3$ 纳米线和电极之间存在的肖特基势垒有关, 表明制备的 $\beta\text{-Ga}_2\text{O}_3$ 纳米线存在表面态缺陷^[156]。而在 265 nm 光照下, 器件光电流迅速增加 3 个数量级, 光暗电流比为 2×10^3 , 最大响应度为 233 A/W。在 200 V 偏压下, 器件的最大光响应度和 EQE 分别为 1680 A/W 和 $8.0 \times 10^5\%$ 。最后, 将器件用于日盲成像, 在 265 nm 光照下器件成像效果明显, 这表明该成像系统对日盲光照具有相对较高的保真度, 在未来日盲光电器件及系统中具有较大的应用潜力。

此外, 由于 $\beta\text{-Ga}_2\text{O}_3$ 存在的特殊晶面, 可以通过机械剥离法从 $\beta\text{-Ga}_2\text{O}_3$ 晶体上剥离准二维纳米薄片, 并将所得结构用于器件制备。2016 年, Oh 等^[72]从 $\beta\text{-Ga}_2\text{O}_3$ 晶体上剥离薄片, 并采用电子束蒸发镀 Cr/Au 电极形成欧姆接触, 制备了基于

$\beta\text{-Ga}_2\text{O}_3$ 薄片的背栅场效应晶体管结构光电探测器。图 4(a)和(b)分别为器件制备流程及器件的光学显微照片。在黑暗环境下, 器件表现出典型的场效应管(FET)特性, $\beta\text{-Ga}_2\text{O}_3$ 沟道层对 254 nm 光照具有较大的光响应[图 4(c)], 同时器件对近紫外光照的响应较小, 在 254 nm 光照下器件的响应度较高(9.17×10^4 A/W), 如图 4(d)、(e)所示。2017 年, 该课题组采用石墨烯电极, 基于剥离的 $\beta\text{-Ga}_2\text{O}_3$ 薄片制备 MSM 结构日盲紫外探测器^[73]。研究发现, 与采用 Ni/Au 电极相比, 在 254 nm 光照下, 基于石墨烯电极的 $\beta\text{-Ga}_2\text{O}_3$ 薄片探测器具有超高光暗比(1.18×10^6), 响应度为 29.8 A/W, 抑制比为 9460, 探测度(D^*)为 1.45×10^{12} Jones。由于石墨烯与半导体之间存在的肖特基势垒在暗环境下阻挡了载流子的扩散, 因此器件暗电流较低, 而石墨烯的高透过率使得 $\beta\text{-Ga}_2\text{O}_3$ 整个区域都可吸收入射光子, 这使得器件光响应较高。

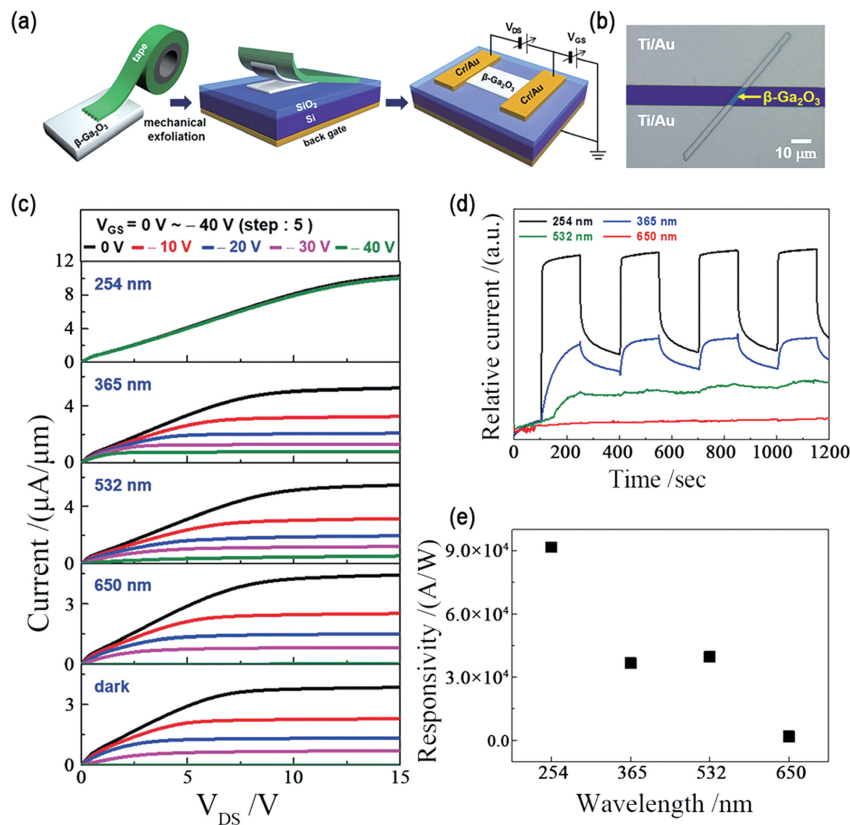


图 4 基于 $\beta\text{-Ga}_2\text{O}_3$ 薄片的器件结构及其电学特性^[72]。(a) $\beta\text{-Ga}_2\text{O}_3$ 薄片基日盲探测器的制备过程;(b) 器件的光学显微照片;(c) $\beta\text{-Ga}_2\text{O}_3$ 薄片基 FETs 的典型电学特性;(d) 器件在不同波长光照下的时间响应;(e) 响应度与波长的函数关系

Fig. 4 Structure and electrical characteristics of the device based on $\beta\text{-Ga}_2\text{O}_3$ flake^[72].(a) Schematic of the preparation process of the $\beta\text{-Ga}_2\text{O}_3$ flake based solar-blind photodetector; (b) optical microscopy image of the device; (c) typical electrical properties of the $\beta\text{-Ga}_2\text{O}_3$ flake based FETs; (d) time-dependent photoresponse of the photodetector under illumination at different wavelengths; (e) responsivity as a function of wavelength

整体来看,虽然已有较多对基于 Ga_2O_3 纳米材料的日盲探测器的研究报道,但 Ga_2O_3 纳米材料器件的研究仍处于初级阶段,与实际应用还有一定距离,有许多问题亟待解决:1)应考虑如何精确控制 Ga_2O_3 纳米材料的尺寸及形貌结构;2)降低 Ga_2O_3 纳米材料的表面态,通过掺杂调控材料的缺陷态,合成具有优异物理化学特性的 Ga_2O_3 纳米材料;3)从实际应用的角度出发,应开发普遍适用的方法以提高具有良好排列和均匀分布的 Ga_2O_3 纳米材料的产量,这对于研制高性能器件至关重要。此外,还需设计与传统光电探测器兼容的新颖光电组件,这是提高器件集成度的一种有效途径。

5.2 Ga_2O_3 单晶日盲紫外探测器

自 2012 年日本研究人员首次将 $\beta\text{-}\text{Ga}_2\text{O}_3$ 单晶衬底用于场效应晶体管以来^[55],基于 $\beta\text{-}\text{Ga}_2\text{O}_3$ 单晶衬底的晶体管性能在过去十余年里取得突破性

进展^[157-161]。而在日盲紫外探测器方面,研究人员对基于 $\beta\text{-}\text{Ga}_2\text{O}_3$ 单晶衬底日盲探测器的相关报道也越来越多,这些器件往往具有较高响应度、快速响应速度等优异性能。2008 年,Oshima 等^[142]基于浮区法生长的 $\beta\text{-}\text{Ga}_2\text{O}_3$ 单晶衬底制备垂直结构日盲紫外探测器,图 5(a)给出了器件制备过程。在暗环境下,器件整流比超过 10^6 (± 3 V),对 200~260 nm 波长的光照射的响应度高达 $2.6\sim 8.7 \text{ A/W}$ [图 5(b)、(c)],较高的响应度是由界面处载流子倍增导致。2009 年,该课题组基于 $\beta\text{-}\text{Ga}_2\text{O}_3$ 单晶制备了火焰检测器[图 5(d)]^[162]。如图 5(e)所示,在 10 Hz 斩波频率下,器件响应速度较快(9 ms)。最后将该器件用于火焰检测系统,当火焰打开时,探测系统能检测到明显的光响应信号[图 5(f)],该结果较好地验证了 $\beta\text{-}\text{Ga}_2\text{O}_3$ 基日盲探测器的实际探测效果。

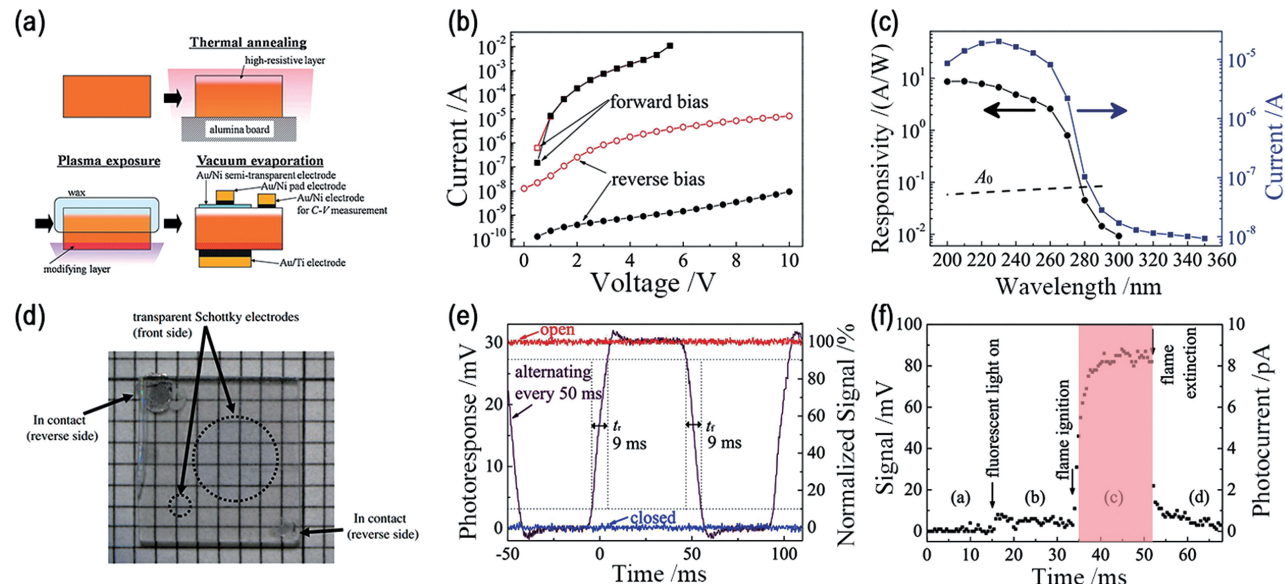


图 5 Ga_2O_3 光电探测器及其性能检测。(a)探测器的制备过程^[142]; (b)器件的电流-电压($I\text{-}V$)特性; 实心和空心点分别表示在黑暗和 250 nm 光照条件下的电流^[142]; (c)在反向 10 V 偏压下器件的光谱响应及响应电流^[142]; (d)火焰探测器的实物图^[162]; (e)探测器的瞬态响应^[162]; (f)来自火焰探测系统的信号^[162]

Fig. 5 Ga_2O_3 photodetector and its performance test. (a) Fabrication process of photodetector^[142]; (b) current-voltage ($I\text{-}V$) characteristics of photodetector. Filled and hollow dots represent current in the dark condition and 250 nm-light irradiation, respectively^[142]; (c) responsivity and photocurrent response of the photodetector at reverse bias of 10 V^[142]; (d) photograph of the flame detector^[162]; (e) transient response of the detector^[162]; (f) signal from the flame detection system^[162]

2009 年,Suzuki 等^[18]在(010)取向 $\beta\text{-}\text{Ga}_2\text{O}_3$ 单晶衬底背面镀较大面积的 Ti/Al(20 nm/100 nm)电极,在衬底正面镀直径约为 1 mm 的 Au 电极(10 nm 厚)形成肖特基接触[图 6(a)插图]。图 6(a)显示了器件的 $I\text{-}V$ 特性,制备的器件表现出较好的整流特性,且退火使得二极管的正向开启电压降低。此外,在 1 V

偏压下,当退火温度超过 200 °C 时,器件整流比从 10^3 增加到 10^6 。在 200~260 nm 波长范围内器件响应度较大,且在 400 °C 退火条件下,器件响应度高达 10^3 A/W [图 6(b)]。

2017 年,Mu 等^[163]通过导模法生长 $\beta\text{-}\text{Ga}_2\text{O}_3$ 单晶并剥离单晶薄片,获得的薄片表面较光滑

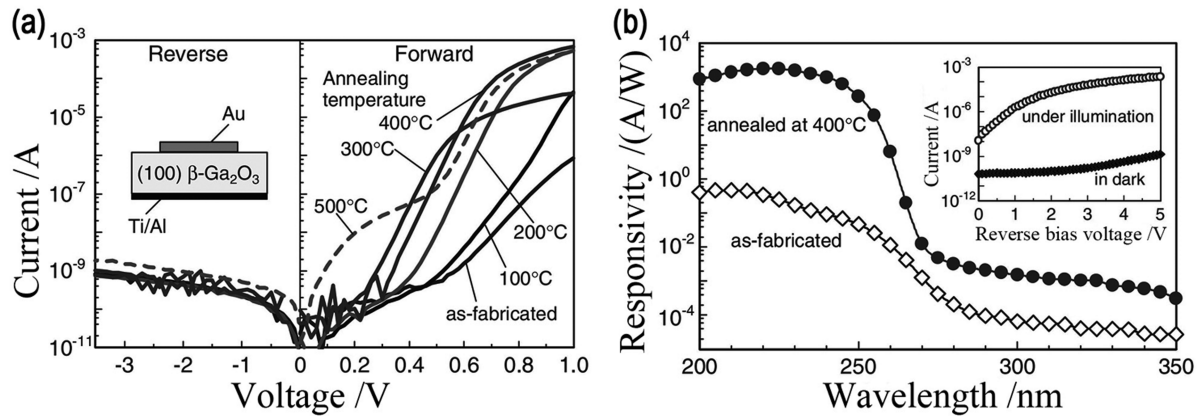


图 6 Ga_2O_3 肖特基二极管的器件性能^[18]。(a)不同温度下退火的 $\text{Au}-\text{Ga}_2\text{O}_3$ 肖特基光电二极管的暗 $I-V$ 特性;(b)退火前后的光谱响应

Fig. 6 Performance of the Ga_2O_3 Schottky photodiode^[18]. (a) Dark $I-V$ characteristics of the $\text{Au}-\text{Ga}_2\text{O}_3$ Schottky photodiode annealed at various temperatures; (b) spectral response of the device before and after annealing

(RMS 为 $0.043\sim0.1 \text{ nm}$),如图 7(a)、(b)所示。随后他们在单晶表面镀 Ti/Au 叉指电极,制备日盲紫外探测器。器件在“开”和“关”循环光照下具有明显的光响应[图 7(c)]。2018 年,该课题组基于 $\beta\text{-}\text{Ga}_2\text{O}_3$ 晶体制备场效应晶体管,用于日盲紫外探测^[164]。漏电压 $V_d=20 \text{ V}$ 时,晶体管的开/关电流比为 2.3×10^6 ,阈值电压约为 -7 V 。计算发现沟

道陷阱密度约为 $2.06\times10^{12} \text{ cm}^{-2}$,这是导致器件具有高阈值电压的原因^[165]。此外,器件光电流随 V_d 呈线性增加,且暗电流达 10^{-12} A ,光电流为 $7.93 \mu\text{A}$, R 为 $4.79\times10^5 \text{ A/W}$,探测度为 $6.69\times10^{14} \text{ Jones}$,EQE 为 $2.34\times10^6 \%$ 。在漏电压 $V_d=20 \text{ V}$ 、栅电压 $V_g=-20 \text{ V}$ 条件下,器件响应时间小于 25 ms,具有较快的响应速度。

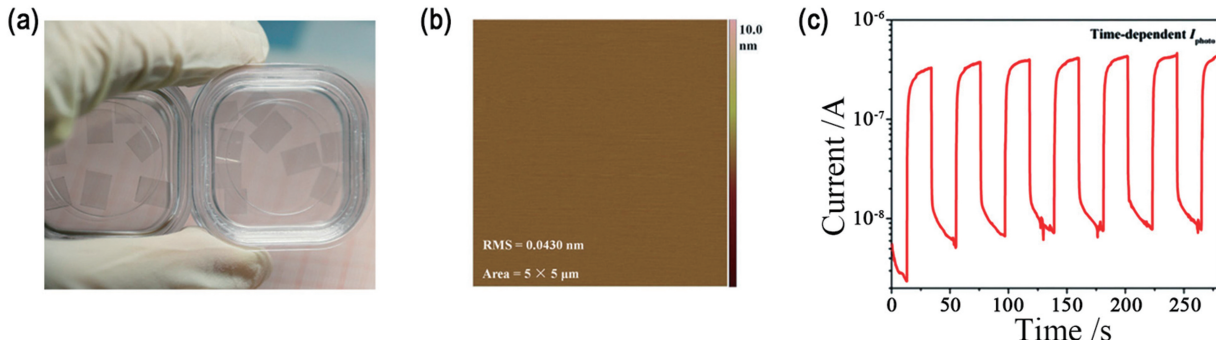


图 7 Ga_2O_3 晶片和器件的时间响应^[163]。(a)(b) Ga_2O_3 外延片及其 AFM 图像;(c)MSM 结构光电探测器的时间响应;

Fig. 7 Crystal wafer of Ga_2O_3 and time response of the device^[163]. (a)(b) Epitaxial wafer and AFM image of the $\beta\text{-}\text{Ga}_2\text{O}_3$; (c) time response of the photodetector with the $\beta\text{-}\text{Ga}_2\text{O}_3$ MSM structure

2019 年,Chen 等^[166]通过在非故意掺杂的(100)面 $\beta\text{-}\text{Ga}_2\text{O}_3$ 单晶上沉积 Pt/Au 电极,制备 MSM 结构光电探测器, $\beta\text{-}\text{Ga}_2\text{O}_3$ 单晶表面粗糙度约为 0.036 nm [图 8(a)]。光电探测器与滤光片[相同的(100)面 $\beta\text{-}\text{Ga}_2\text{O}_3$ 单晶]的 b 轴正交排列($b_{\text{detector}} \perp b_{\text{filter}}$)时产生窄带探测[图 8(b)],偏振光垂直于 b 轴时,262 nm 处的 R 为 0.23 A/W ,响应带宽约为 10 nm ,这可确保较小的杂散背景信号。在 8 Hz 斩波频率下,器件 UVC-UVA 抑制比超过 800 ,EQE 为 110% ,随着入射光调制频率的增加,窄带宽未发生改变,而响应度峰值逐渐降低

[图 8(c)]。图 8(d)显示了日盲探测器在 5 V 偏压下的时间响应谱,可以看出器件对 266 nm 脉冲激光(光功率密度为 1.5 mW/cm^2)具有较短的响应时间(上升、下降时间为 0.48 ms 和 0.38 ms)。

综上所述,通过改善器件结构等方法,基于 Ga_2O_3 单晶的日盲探测器的性能已经得到了较大提升,但制备大直径、高质量的 Ga_2O_3 单晶仍是一项重要挑战。单晶内部位错等缺陷的形成机制研究对生长大尺寸、高质量 Ga_2O_3 单晶及制备高性能器件具有重要意义,但是目前关于单晶内部位错等缺陷的形成机制的研究较少。此外,如何设计新型器

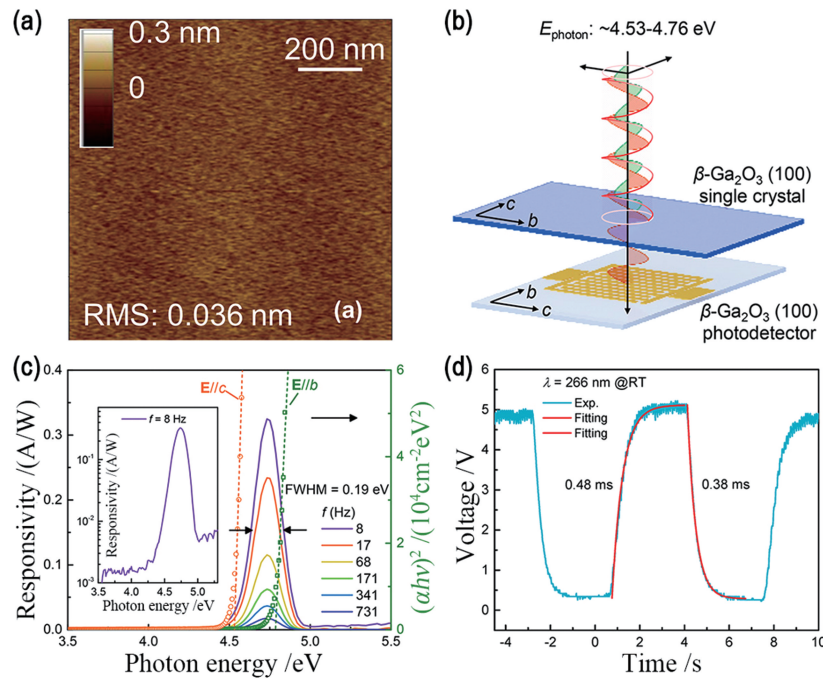


图 8 $\beta\text{-Ga}_2\text{O}_3$ 单晶窄带探测器的结构及其光响应^[166]。(a)(100)面 $\beta\text{-Ga}_2\text{O}_3$ 单晶的 AFM 图像;(b)窄带探测器与正交对准滤波器的组合结构;(c)光响应度随斩波调制频率的变化;(d)在 150 Hz 下测得的瞬态光响应波形曲线的拟合

Fig. 8 Configuration and its photoresponse of the narrow-band detector based on $\beta\text{-Ga}_2\text{O}_3$ single crystal^[166]. (a) AFM image of the (100) $\beta\text{-Ga}_2\text{O}_3$ single crystal; (b) configuration of the narrow-band detector combined with an orthogonally aligned filter; (c) photoresponsivity as a function of chopper modulation frequency; (d) fitting of waveform curves of transient photoresponse measured at 150 Hz

件结构以确保器件的可靠性仍然是目前研究工作中面临的主要问题。

5.3 Ga_2O_3 薄膜日盲紫外探测器

2011 年, Weng 等^[167]采用 MOCVD 制备 GaN 薄膜并通过氧化方法获得 $\beta\text{-Ga}_2\text{O}_3$ 薄膜, 最后通过在薄膜表面镀 Ti/Al/Ti/Au 电极制备日盲紫外探测器[图 9(a)]。在 5 V 偏压下, 器件的暗电流为 $1.39 \times 10^{-10} \text{ A}$, 在紫外光照下, 电流增加到 $2.03 \times$

10^{-5} A , 开/关电流比约为 10^5 [图 9(b)]。此外, 器件对 260 nm 光照的响应度为 0.453 A/W 。

2011 年, Suzuki 等^[168]在(100)面 $\beta\text{-Ga}_2\text{O}_3$ 单晶衬底上采用溶胶-凝胶法制备 $\beta\text{-Ga}_2\text{O}_3$ 覆盖层并制备日盲光电二极管[图 10(a)]。无论二极管有无覆盖层, 器件均表现出明显的整流特性, 且在正向偏压下, 有 $\beta\text{-Ga}_2\text{O}_3$ 覆盖层的器件的开启电压为 5.4 V (无覆盖层器件的开启电压为 1.6 V), 电阻为 $15 \text{ k}\Omega$

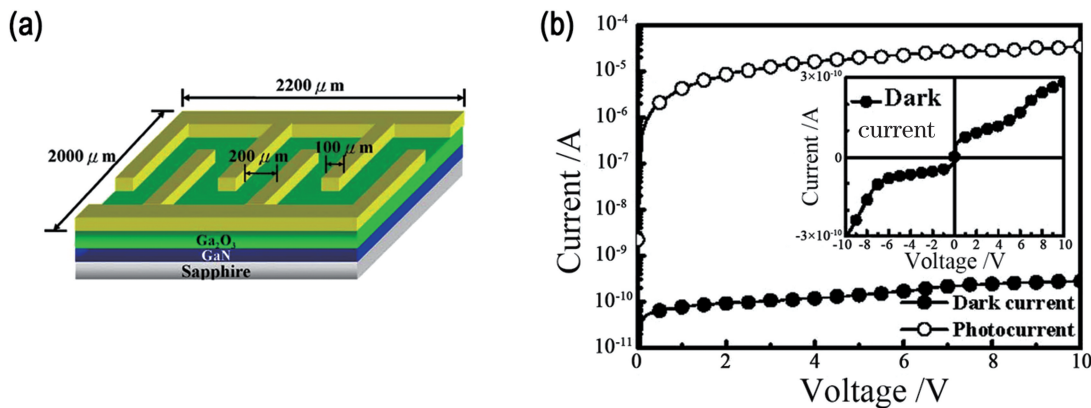


图 9 制备的光电探测器示意图和测试的 $I\text{-}V$ 特性曲线^[167]。(a)制备的光电探测器示意图;(b)测试的 $I\text{-}V$ 特性曲线

Fig. 9 Schematic diagram and measured $I\text{-}V$ characteristic curves of the fabricated $\beta\text{-Ga}_2\text{O}_3$ photodetector. (a) Schematic diagram of the fabricated $\beta\text{-Ga}_2\text{O}_3$ photodetector; (b) measured $I\text{-}V$ characteristic curves

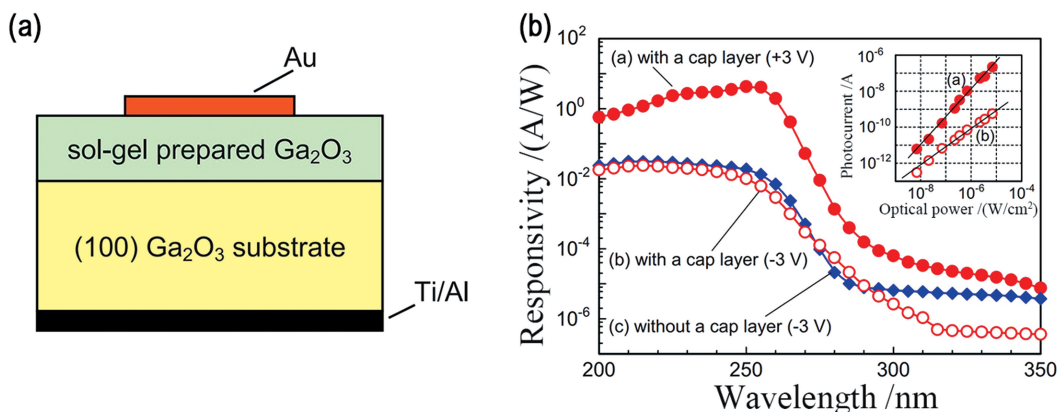


图 10 器件结构示意图及其光谱响应^[168]。(a) β -Ga₂O₃ 单晶光电二极管的结构示意图;(b)有/无覆盖层的 Ga₂O₃ 光电二极管在 3 V 反向和正向偏压下的光谱响应

Fig. 10 Structural schematic of the device and its spectral response^[168]. (a) Structural schematic of β -Ga₂O₃ single-crystal photodiode; (b) spectral response of Ga₂O₃ photodiodes with and without a cap layer at reverse and forward biases of 3 V

(无覆盖层器件的电阻为 10 Ω),这说明溶胶-凝胶制备的 β -Ga₂O₃ 覆盖层在器件中相当于一个高阻层。图 10(b)显示了器件的光谱响应,可以看出具有 β -Ga₂O₃ 覆盖层的二极管在正偏和反偏条件下对 200~260 nm 波段的日盲光照均有较强的光响应。

2015 年, Hu 等^[169]采用 MOCVD 在 c 面蓝宝石衬底上沉积 β -Ga₂O₃ 薄膜,随后通过在薄膜表面镀 Au 电极(间距为 10 μm)制备日盲紫外探测器,器件响应度为 17 A/W,截止波长为 260 nm,同时紫外-可见光抑制比($R_{255 \text{ nm}}/R_{450 \text{ nm}}$)为 8.5×10^6 。当电压超过 6 V 时,响应度急剧增加。在 20 V 偏压下,器件 EQE 达到 8228%,探测度为 7.0×10^{12} Jones,由来自 Au 电极与 Ga₂O₃ 覆盖区域中的载流子倍增导致的内部增益是器件具有高响应度和高量子效率的主要原因。此外,Liu 等^[96]通过 MBE 沉积带有同质自模板缓冲层的高质量 β -Ga₂O₃ 薄膜(半峰全宽约为 0.55°),并通过采用电子束蒸发在薄膜表面镀 Ti/Au 电极制备日盲探测器。在 20 V 偏压、13 mW/cm² 光照条件下,器件的光电流为 438 nA,响应度为 259 A/W,光暗电流比为 10⁴,外量子效率为 $7.9 \times 10^4\%$,器件在 235 nm 处的响应度比 400 nm 处高三个数量级,具有较高的日盲光电特性。

由于掺杂可以有效调控 Ga₂O₃ 的电导率^[170],因此研究人员针对不同掺杂元素对 Ga₂O₃ 薄膜日盲紫外探测器的光电性能的影响进行了研究^[60, 122, 171-174]。2016 年,Wu 等^[171]采用射频磁控溅射在(0001)蓝宝石衬底上制备不同 Er³⁺ 掺杂浓度(原子数分数)的 β -Ga₂O₃ 薄膜并基于薄膜制备日盲探测器。随着 Er³⁺ 掺杂浓度的增加,薄膜 PL

发射峰强度逐渐增加[图 11(a)],制备的器件在 20 V 偏压下的暗电流为 0.8 nA,同时器件对 365 nm 光照无响应。在对激光分子束外延(LMBe)沉积的 ϵ -Ga_{1.8}Sn_{0.2}O₃ 薄膜的研究工作中,薄膜带隙随着 Sn⁴⁺ 离子掺入 Ga³⁺ 位点而略微减小^[172]。在暗环境下, ϵ -Ga_{1.8}Sn_{0.2}O₃ 薄膜器件具有较低的电导率,但器件对 254 nm 光照具有明显的光响应。此外,当引入 Zn 掺杂时, β -Ga₂O₃ 薄膜晶格畸变随 Zn 掺杂浓度的增加而增加,且 V_o 浓度降低^[122];与纯 β -Ga₂O₃ 薄膜器件相比,Zn : β -Ga₂O₃ 薄膜日盲探测器具有更高的光暗电流比,响应速度更快。而 Mg 元素掺杂会使 β -Ga₂O₃ 薄膜的费米能级更接近价带,薄膜表现出弱 p 型导电^[60];制备的日盲探测器在 10 V 偏压下的暗电流为 4.1 pA,比未掺杂薄膜器件低三个数量级,器件灵敏度($I_p - I_d$)为 $8.7 \times 10^5\%$ 。Ce 掺杂 β -Ga₂O₃(Ce : β -Ga₂O₃)薄膜的 PL 谱出现紫外、蓝光和绿光三个发射峰[图 11(b)],当 Ce 浓度增加到 1.0% 时,PL 发射强度达到最大,随后由于浓度淬灭效应,发射峰强度降低,制备的 Ce(浓度为 0.7%) β -Ga₂O₃ 薄膜探测器对 254 nm 光照具有较强的光响应^[174]。此外,美国研究人员 Alema 等^[62]于 2017 年通过 MOCVD 技术生长 Zn($\sim 5 \times 10^{20} \text{ cm}^{-3}$)掺杂 β -Ga₂O₃ 薄膜(ZnGaO)并制备日盲探测器。薄膜在 O₂ 中退火后,制备的日盲探测器暗电流从 \sim nA 降到 \sim pA 范围,在 20 V 偏压下,器件响应度为 210 A/W(波长为 232 nm), $R_{232 \text{ nm}}/R_{320 \text{ nm}}$ 为 5×10^4 。

2017 年,Cui 等^[139]通过射频磁控溅射在不同氧分压下分别在柔性和石英衬底上沉积非晶 Ga₂O₃ 薄膜,并在薄膜表面镀 ITO 电极以制备 MSM 结构

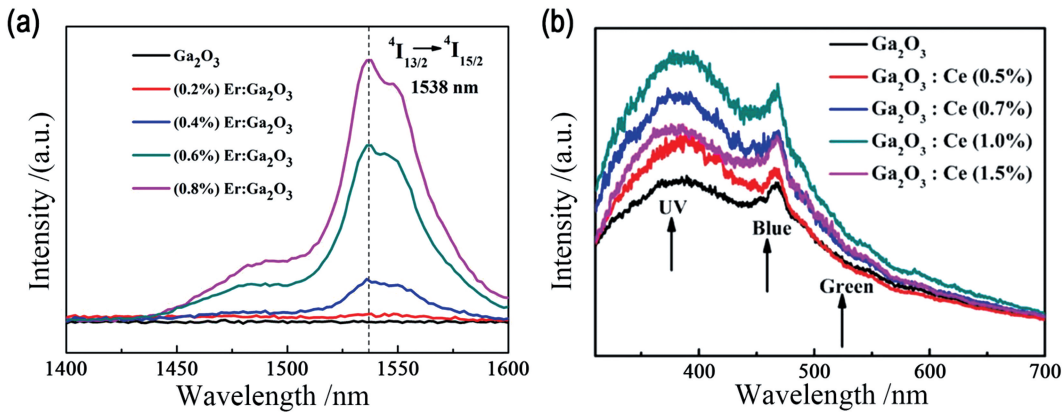


图 11 Ga₂O₃ 薄膜的 PL 谱。(a) 不同浓度 Er : Ga₂O₃ 薄膜的近红外光致发光谱^[171]; (b) 不同掺杂浓度 Ce : Ga₂O₃ 薄膜的 PL 谱^[174]

Fig. 11 PL spectra of Ga₂O₃ films. (a) NIR PL spectra of Er : Ga₂O₃ films with different concentrations^[171];
(b) PL spectra of Ce : Ga₂O₃ films with different doping concentrations^[174]

的日盲紫外探测器。在 10 V 偏压下,器件暗电流为 0.2 μA,随着氧分压的增加,由于界面处势垒高度的增加,器件暗电流明显降低^[175],此外,器件的光暗电流比较大(>10⁴),响应时间较短(19.1 μs)。在 Huang 等^[176]报道的不同氧分压下生长 β-Ga₂O₃薄膜的工作中,V_O浓度随氧分压的增加而降低,而过高氧分压会导致器件光电流降低,这与 V_O、V_{Ga} 和 V_O-V_{Ga} 复合体缺陷对光生载流子的捕获有关^[177]。2017 年,Qian 等^[178]分别采用射频磁控溅射和 MBE 沉积非晶 Ga₂O₃(a-Ga₂O₃)和晶体 β-Ga₂O₃薄膜,并通过镀 Ti/Al 叉指电极制备 MSM 结构日盲紫外探测器。研究发现 a-Ga₂O₃ 薄膜存在的大量缺陷态使得薄膜与电极形成欧姆接触且暗电流较大(338.6 pA)^[179],而晶体 β-Ga₂O₃ 薄膜由于缺陷减少,器件暗电流较低(9.7 pA)。此外,基于 a-Ga₂O₃ 和 β-Ga₂O₃ 薄膜的器件均对日盲光照有明显响应,但相比之下 a-Ga₂O₃ 薄膜器件的响应度较高(70.26 A/W),这归因于薄膜内部增益机制和缺陷态对少数载流子的捕获^[180-181]。

2018 年,Xu 等^[182]采用 Mist-CVD 方法在蓝宝石衬底上生长 β-Ga₂O₃ 薄膜,蓝宝石衬底温度分别被加热到 400, 470, 550, 600 °C, 随后通过镀 Al 制备 MSM 结构的日盲紫外探测器。在 20 V 偏压下,器件暗电流为 14 pA,光暗电流比超过 10⁵,低暗电流表明器件具有较高的灵敏度且噪声较小^[183]。在 550 °C 下制备的薄膜器件在 254 nm 光照、20 V 偏压下的响应度为 150 A/W,EQE 为 7.39 × 10⁴ %。2019 年,Chen 等^[138]报道了基于非晶 Ga₂O₃ 薄膜的 3D 日盲探测器阵列。该器件具有较高的光暗电流

比(10⁴)和探测度(3.3 × 10¹³ Jones),该 3D 探测器阵列实现了实时光轨迹和多点分布的检测。

2019 年,Qiao 等^[184]通过 MOCVD 技术生长 β-Ga₂O₃ 薄膜并制备了 MSM 结构的光电二极管探测器。器件在 365 nm 光照下的光电流仅为 3.1 pA, R_{254 nm}/R_{365 nm} 超过 10⁷[图 12(a)],在 254 nm 光照下,器件的探测度为 9.8 × 10¹⁵ Jones,EQE 为 2.3 × 10⁴ %,光生载流子在电极下方高场区域形成的载流子雪崩倍增使得器件性能较突出。在最近报道的工作中,Han 等^[185]通过化学刻蚀方法制备非晶 Ga₂O₃ 薄膜晶体管,当源漏电压 V_{DS} 从 0.1 V 增加到 10 V 时,漏电流 I_{DS} 逐渐增加,且 I_{DS} 在较低水平(10⁻¹² A)。当源漏电压 V_{DS} = 10 V、源栅电压 V_{GS} = 4 V 时,器件光电流约为 10⁻⁴ A,光暗电流比高达 5 × 10⁷。在紫外光照下,电子从价带被激发到导带,并且深能级中性 V_O 缺陷被离化为浅施主 V_O²⁺ 或 V_O⁺,这两者都对源极和漏电极之间流动的电流有较大贡献^[186-187]。由于存在大量的光生电子,在黑暗环境下耗尽区“关闭”态会反转为“开启”态,因此器件具有超高的抑制比^[188]。在 V_{DS} = 10 V 的条件下,器件响应度为 5.67 × 10³ A/W,探测度为 1.87 × 10¹⁵ Jones;通过控制栅电压(20 V)实现了对持续光电导效应的有效控制,晶体管响应速度较快(5 ms)。此外,Qin 等^[136]报道了 ε-Ga₂O₃ 薄膜基 MSM 结构的日盲紫外探测器。实验通过 MOCVD 技术在蓝宝石衬底上外延 1 μm 厚 ε-Ga₂O₃ 薄膜,并在薄膜表面镀 20 nm/50 nm 厚 Ti/Au 叉指电极以制备日盲探测器。随着测试温度的升高,器件暗电流逐渐增加[图 12(b)],这表明金属-半导体(MS)

整体或界面缺陷对电流传输具有较大影响^[189-190]。在低电压区域,器件暗电流随电压的增加呈指数增加,而在高电压区域,暗电流随电压的变化产生较小的变化,因此,暗电流在低电压区域的传输机制主要以热电子发射为主。在 6 V 偏压下,器件的光暗电流比为 1.7×10^5 ,具有较高的信噪比, $R_{250\text{ nm}}/R_{400\text{ nm}}$

为 1.2×10^5 ,EQE 为 $1.13 \times 10^5\%$ [图 12(c)]。此外,图 12(d)给出了器件的电流-时间($I-t$)曲线的下降沿放大图,由于 $\epsilon\text{-Ga}_2\text{O}_3$ 薄膜中较低的缺陷浓度,器件下降时间较快(24 ms/79 ms)。理论计算和阴极发光谱表明,金属/半导体界面处的深能级受主捕获状态对光电流起主要贡献作用并导致较大的增益。

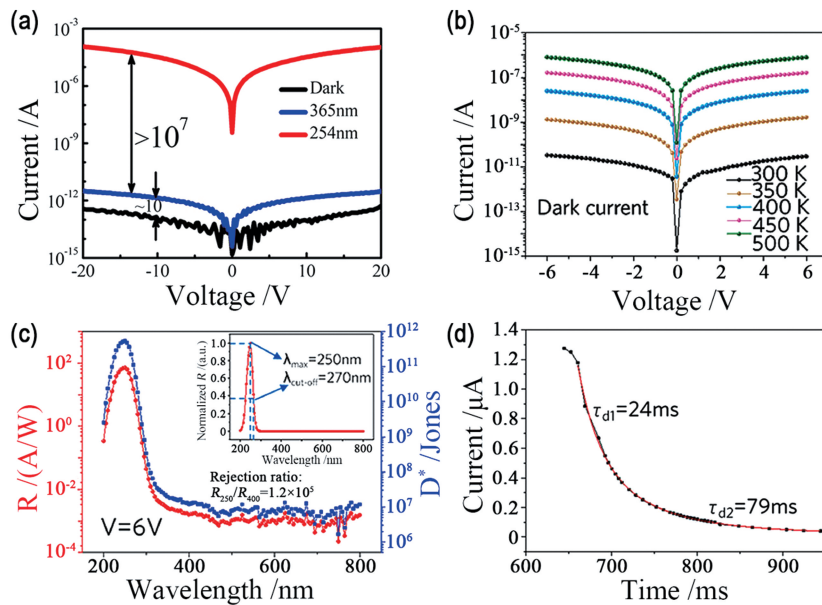


图 12 Ga_2O_3 日盲探测器的电学特性和光谱响应。(a) 800 °C 退火薄膜的 $I-V$ 特性^[184]; (b) MSM $\epsilon\text{-Ga}_2\text{O}_3$ 光电探测器在暗环境不同温度下的 $I-V$ 曲线^[136]; (c) MSM $\epsilon\text{-Ga}_2\text{O}_3$ 光电探测器在 6 V 偏压下 R 和 D^* 与波长的关系^[136]; (d) $I-t$ 特性曲线下降沿放大图^[136]

Fig. 12 Electrical characteristics and spectral response of Ga_2O_3 solar-blind photodetectors. (a) $I-V$ characteristics of the annealed $\beta\text{-Ga}_2\text{O}_3$ thin film at 800 °C^[184]; (b) $I-V$ curves of the MSM $\epsilon\text{-Ga}_2\text{O}_3$ photodetector in the dark at variable temperatures^[136]; (c) R and D^* as functions of the wavelength of the MSM $\epsilon\text{-Ga}_2\text{O}_3$ photodetector at a bias of 6 V^[136]; (d) magnified fall edge of the $I-t$ characteristic curves^[136]

表 3 基于 Ga_2O_3 薄膜的光电探测器的性能参数汇总

Table 3 Summary of parameters of Ga_2O_3 thin films based photodetectors

Growth Method	Material	I_d / nA	R / ($\text{A} \cdot \text{W}^{-1}$)	EQE / %	t_r / s	t_d / s	Ref. No	Year
	$\beta\text{-Ga}_2\text{O}_3$ film	128	—	—	0.86	1.02	[94]	2014
	$\beta\text{-Ga}_2\text{O}_3$ film	45	—	—	0.62	0.83	[183]	2014
	$\beta\text{-Ga}_2\text{O}_3$ film	0.04	259	$>10^4$	0.4	0.1	[96]	2015
MBE	$\beta\text{-Ga}_2\text{O}_3$ film	842.1	0.07	36	0.91	0.28	[191]	2016
	$\beta\text{-Ga}_2\text{O}_3$ film	70	153	—	5	10.3	[192]	2017
	$\beta\text{-Ga}_2\text{O}_3$ film	10	1.5	—	3.3	0.4	[5]	2017
	$\beta\text{-Ga}_2\text{O}_3$ film	0.026	54.9	—	2	4	[193]	2017
	$\beta\text{-Ga}_2\text{O}_3$ film	7.3	10^{-5}	0.5	—	—	[194]	2018
	$\beta\text{-Ga}_2\text{O}_3$ film	—	8.41	—	2.97	0.41	[195]	2019

续表3

Growth Method	Material	I_d / nA	R / (A · W ⁻¹)	EQE / %	t_r / s	t_d / s	Ref. No	Year
RFMS	β -Ga ₂ O ₃ film	40	43.31	>10 ⁴	1.08	0.65	[121]	2017
	Ga ₂ O ₃ film	0.34	70.26	—	0.41	0.02	[178]	2017
	Mg : β -Ga ₂ O ₃ film	~10 ⁻³	0.024	—	0.33	0.02	[60]	2017
	Ga ₂ O ₃ film	—	0.19	—	<10 ⁻⁵	<10 ⁻⁵	[139]	2017
	β -Ga ₂ O ₃ film	10 ⁻³	0.893	444	0.31	0.25	[137]	2018
	β -Ga ₂ O ₃ film	7.63	2.602	1265	0.26	1.00	[124]	2018
	Ga ₂ O ₃ film	~10 ⁻³	436.3	—	~10 ⁻⁸	~10 ⁻⁴	[196]	2019
	Ga ₂ O ₃ film	16300	55.5	—	—	~10 ⁻⁴	[197]	2019
PLD	β -Ga ₂ O ₃ film	~10 ⁻²	144.46	64711	~10 ⁻⁸	~10 ⁻⁵	[144]	2019
	Ga ₂ O ₃ film	0.17	8.9	4450	—	~10 ⁻³	[138]	2019
	β -Ga ₂ O ₃ film	~10 ⁻³	3.7	—	—	—	[198]	2018
MOCVD	β -Ga ₂ O ₃ film	2.5	0.33	—	~10 ⁻⁶	<10 ⁻⁴	[199]	2018
	β -Ga ₂ O ₃ film	2.82	0.415	197.8	—	—	[200]	2019
	β -Ga ₂ O ₃ film	34	26.1	>10 ⁴	0.48	0.18	[201]	2017
	Zn : β -Ga ₂ O ₃ film	10	>10 ³	—	4.5	0.8	[62]	2017
	β -Ga ₂ O ₃ film	12.8	12.8	—	~10 ⁻³	~10 ⁻³	[115]	2018
ALD	β -Ga ₂ O ₃ film	~10 ⁻⁴	150	>10 ⁴	1.8	0.3	[182]	2018
	Zn : Ga ₂ O ₃ film	~10 ⁻⁴	1.05	512	4.5	2.2	[202]	2018
	Mg : Ga ₂ O ₃ film	0.52	8.9	4341	0.16	0.14	[103]	2019
	β -Ga ₂ O ₃ film	—	46	>10 ⁴	~10 ⁻⁶	~10 ⁻⁵	[184]	2019
	ϵ -Ga ₂ O ₃ film	0.023	230	>10 ⁵	—	0.024	[136]	2020
	β -Ga ₂ O ₃ film	~10 ⁻³	3930.55	92879	0.195	0.091	[203]	2020
	β -Ga ₂ O ₃ film	0.2	45.11	—	~10 ⁻⁶	—	[110]	2017
	α -Ga ₂ O ₃ film	~10 ⁻³	0.76	—	~10 ⁻⁷	<10 ⁻⁴	[204]	2018
	α -Ga ₂ O ₃ film	0.163	1.2	—	—	—	[205]	2019
	Ga ₂ O ₃ film	~0.01	1.34	—	—	~10 ⁻⁷	[206]	2020

表3总结了基于不同制备方法生长的Ga₂O₃薄膜日盲紫外探测器的各项参数指标。从表中可以看出,MOCVD制备的 β -Ga₂O₃薄膜日盲探测器具有较低的暗电流(10^{-4} nA),通过掺杂也可有效降低暗电流^[182,202]。其次,将射频磁控溅射沉积的 β -Ga₂O₃薄膜用于日盲探测器阵列时器件暗电流较低,Mg掺杂制备的弱p型导电 β -Ga₂O₃薄膜的暗电流达到pA量级^[60,137]。而MOCVD制备的 β -Ga₂O₃薄膜光电二极管也具有较高响应度(3930.55 A/W),同时量子效率较高(92879%)^[203]。此外,基于射频磁控溅射沉积的Ga₂O₃薄膜的光电二极管量子效率同样能达到较高水平(64711%),且响应速度较快^[144],MOCVD

外延生长的 ϵ -Ga₂O₃薄膜制备的MSM结构的日盲探测器具有超高量子效率(>10⁵%)^[136],沉积在SiC衬底上的 β -Ga₂O₃薄膜日盲探测器也具有较高量子效率^[124];而通过ALD沉积的Ga₂O₃薄膜用于MSM结构的日盲探测器时器件往往表现出较快的响应速度^[110,204,206]。

与Ga₂O₃纳米结构及单晶相比,Ga₂O₃薄膜的制备工艺较成熟且目前技术可以沉积大面积高质量的Ga₂O₃薄膜,同时研究人员对基于Ga₂O₃薄膜的日盲探测器的研究范围更广,通过改善薄膜结晶质量、改进器件结构等方法可以有效提升器件性能。此外,由于Ga₂O₃薄膜日盲探测器存在的高响应度和快速响应不可兼得的问题目前已有较大改善,因

此在未来的研究工作中 Ga_2O_3 薄膜基日盲探测器更有希望应用到实际中。然而, Ga_2O_3 薄膜 p 型导电问题仍是一项重要挑战, 这限制了 Ga_2O_3 薄膜在 p-n 结器件方面的应用。

5.4 Ga_2O_3 异质结日盲紫外探测器

2013 年, Huang 等^[207] 通过 MOCVD 生长 $\beta\text{-Ga}_2\text{O}_3/\text{AlGaN}/\text{GaN}$ 异质结并制备了日盲探测器。在反向偏压下, 有 $\beta\text{-Ga}_2\text{O}_3$ 层的器件暗电流处于更低水平 ($4.7 \times 10^{-10} \text{ A}$); 与之前的工作类似, 在不同偏压下, 器件截止波长出现在不同位置 (UV-C 和 UV-B)。2015 年, Nakagomi 等^[208] 基于 p-GaN 制备 $\beta\text{-Ga}_2\text{O}_3/\text{p-GaN}$ 异质结光电二极管。器件在 4.5 V 偏压下的整流比为 1.5×10^5 ; 在暗环境、-8 V 偏压下, 器件的暗电流低于 10^{-9} A [图 13(a)], 响应度峰值位于 225 nm, 而由于 GaN 的吸收, 器件在 360 nm 附近仍然存在光响应, 同时

器件响应速度与之前的工作相比有较大提升。

2015 年, Guo 等^[209] 通过 LMBE 技术在 p 型 Si 衬底上沉积 $\beta\text{-Ga}_2\text{O}_3$ 薄膜, 制备 $\beta\text{-Ga}_2\text{O}_3/\text{Si}$ p-n 结日盲探测器。器件的光暗电流比为 920, $R_{254 \text{ nm}}$ 为 370 A/W, EQE 为 $1.8 \times 10^5 \%$ 。同年, Zhao 等^[150] 制备了 $\text{ZnO}/\text{Ga}_2\text{O}_3$ 核-壳结构的异质结日盲紫外探测器 [图 13(b)]。器件在反向偏压、254 nm 光照条件下的光电流高于暗电流 $10^3 \sim 10^6$ 量级 [图 13(c)], 在 -10 V 偏压条件下的响应度为 $5.18 \times 10^3 \text{ A/W}$, 外量子效率为 $2.53 \times 10^6 \%$, 器件具有较大的内部增益, 响应截止波长为 266 nm, 该波长对应日盲波段, 如图 13(d) 所示。由于电子亲和能 (χ) 及带隙差异, ZnO 和 Ga_2O_3 之间的电子能量势垒 (ΔE_c) 远大于空穴 (ΔE_v), 这会导致电子发生碰撞电离产生雪崩倍增, 使得器件具有较大的性能参数。

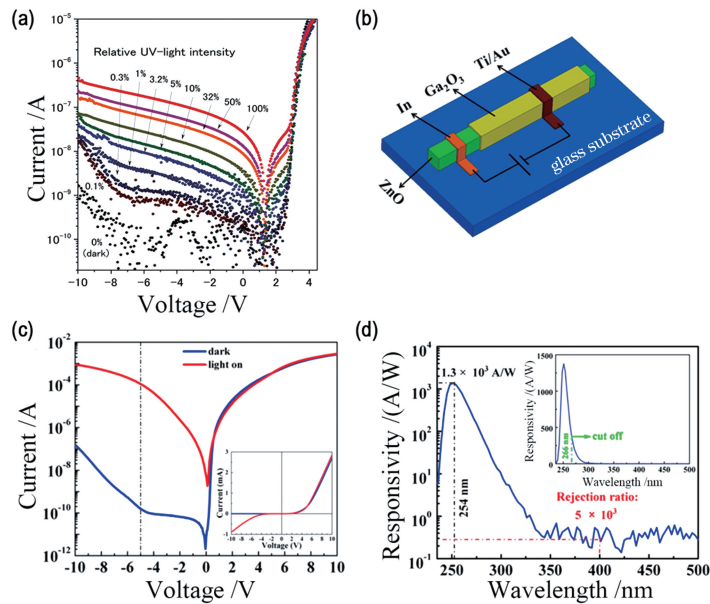


图 13 器件的 I-V 特性及光谱响应。(a) 不同光照下的电流-电压特性^[208]; (b) APD 示意图^[150]; (c) 器件的 I-V 特性^[150]; (d) 器件在 -6 V 偏压下的光谱响应^[150]

Fig. 13 I-V characteristics and spectral response of the device. (a) Current-voltage characteristics for various UV-light illumination intensities^[208]; (b) schematic diagram of the APD^[150]; (c) I-V characteristics of the device^[150]; (d) spectral response of the device at -6 V bias^[150]

2016 年, Mahmoud^[210] 报道了 $\beta\text{-Ga}_2\text{O}_3/\text{SnO}_2$ 异质结雪崩光电探测器 (APD)。探测器在暗环境下的 I-V 特性表现出典型的单结整流特性, 在反向偏压下器件光电流比暗电流大 10^4 倍。光电探测器在 5.5 V 偏压下的雪崩增益为 1.7×10^5 , 在 10 V 偏压下, 器件响应度为 $6.3 \times 10^3 \text{ A/W}$, 抑制比为 7.4×10^3 , 具有较高的光谱选择性。此外, 器件在 254 nm 光照下的 EQE 为 $4.48 \times 10^6 \%$, 且响应速

度较快。同年, 本课题组基于多层石墨烯 (MLG) 和 $\beta\text{-Ga}_2\text{O}_3$ 制备异质结日盲探测器^[211]。在 20 V 偏压下, 器件的响应度和探测度分别为 39.3 A/W 和 $5.92 \times 10^{13} \text{ Jones}$, EQE 为 $1.98 \times 10^4 \%$, 器件的最大响应度位于 220 nm, 波长继续增大时响应度逐渐减小。2017 年, Guo 等^[121] 基于质量分数为 0.7% 的 Nb : SrTiO₃ (NSTO) 和 $\beta\text{-Ga}_2\text{O}_3$ 薄膜制备异质结日盲紫外探测器。器件的暗电流在开启电压为 3 V 后

急剧增加,在 254 nm 光照下,光电流随光照强度的增加而增加,−10 V 偏压下的光暗电流比为 3×10^4 。

2017 年,Chen 等^[212]基于 ZnO 和 α 相 Ga₂O₃ 制备 n-n 异质结日盲探测器。实验通过 LMBE 技术在 ZnO 衬底上沉积 α -Ga₂O₃ 薄膜,探测器衰减过程的快速/慢速响应时间为 563 μ s/12.2 ms [图 14(a)],其中快速衰减由雪崩碰撞电离过程引起,而慢速衰减由光导增益引起^[213]。−10 V 偏压下,器件光电导增益增加到 10^2 ,对应的响应度为 2.1 A/W,而在 10 V 条件下,增益高达 10^4 ,响应度为 1.05×10^3 A/W[图 14(b)]。在 254 nm 光照下,Ga₂O₃ 近表面产生的空穴被迅速扫出,电子被内建电场加速到 ZnO 侧,因此产生的雪崩倍增可视为几乎纯电子注入的碰撞电离过程所导致,如图 14(c)所示。此外,Wang 等^[214]报道了基于非晶和晶体 Ga₂O₃(a/c-Ga₂O₃)薄膜相结日盲探测器。从室温到 750 °C 的射频磁控溅射实验结果显示,当生长温度为 400 °C

时薄膜出现明显的非晶和晶体混合形态[图 14(d)]。制备的器件具有明显的整流特性,光暗电流比大于 10^7 。器件响应时间 τ_r/τ_d 为 0.012/19.6 μ s,抑制比约为 8.1×10^4 ,最大外量子效率约为 400% [图 14(e)、(f)],器件表现出较高的光谱选择性,在探测微弱光信号方面具有较大的应用潜力。2019 年,Nakagomi 等^[149]基于 p 型 4H-SiC 和 β -Ga₂O₃ 制备异质结二极管,用于日盲紫外探测。在 4H-SiC 表面镀 Al/Ti/Al/Pt 电极, β -Ga₂O₃ 表面镀 Ti/Al/Pt/Au 电极, β -Ga₂O₃ 中电子势垒高度和 4H-SiC 中空穴势垒高度分别为 2.57 eV 和 4.21 eV,器件开启电压和串联电阻随温度的升高而逐渐降低。器件在暗环境下的反向饱和电流低于 1×10^{-10} A,相关分析结果表明,当入射光到达薄膜一定厚度处时其强度明显降低,表明 β -Ga₂O₃ 层的厚度对器件反向电流存在影响。此外,二极管的最大响应度位于 260 nm,同时响应速度较快($< 30 \mu$ s)。

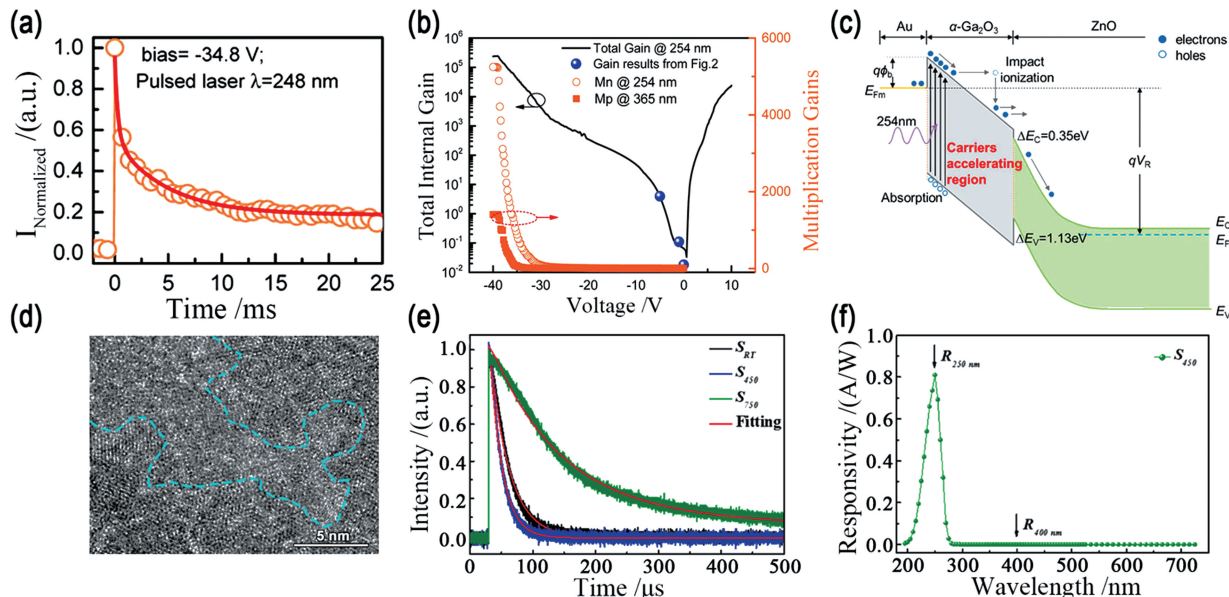


图 14 器件的光响应原理和光谱响应。(a) 室温下的归一化瞬态光响应特性^[212]; (b) 器件的光电导增益及雪崩倍增与偏压的关系^[212]; (c) 在高反偏压和 254 nm 光照下的能带示意图^[212]; (d) 从样品得到的 HRTEM 图像^[214]; (e) Ga₂O₃ 薄膜探测器脉冲电流与时间的函数关系^[214]; (f) 器件在 5 V 偏压下的光谱响应^[214]

Fig. 14 Principle of photoresponse and spectral response of the device. (a) Normalized transient photoresponse characteristics at room temperature^[212]; (b) photoconductive gain and avalanche multiplication gain for the device as functions of applied bias^[212]; (c) energy band diagram at high reverse bias under 254 nm illumination^[212]; (d) HRTEM images acquired from sample^[214]; (e) pulse photocurrent as a function of the time of the Ga₂O₃ thin-film photodetectors^[214]; (f) spectral responsivity of the device at bias of 5 V^[214]

5.5 Ga₂O₃ 基自驱动日盲紫外探测器

众所周知,传统光电导型日盲探测器往往需要提供外部电源以驱动其正常工作。然而,这种能量负载使得器件体积变大,同时还需保证能量源的不

间断供应,这使得器件在实际应用中受到较大限制。近年来,国内外研究人员正在构建基于光伏效应的自驱动日盲探测器件,该器件可以从环境中获取能量并可独立可持续运行,这大大降低了对传统能源

供应的依赖性^[215-219]。与光电导型器件相比,光伏型自驱动探测器主要由 p-n 结、异质结或肖特基结制成,器件往往表现出更高的灵敏度、更大的响应速度及更低的暗电流。自驱动探测器的主要机制为光生伏特效应,首先器件吸收入射光子产生电子-空穴对,在内建电场作用下光生电子-空穴对被快速分离,最后通过外电路收集光生载流子^[220-221]。 $\beta\text{-Ga}_2\text{O}_3$ 具有本征 n 型导电性,可以结合其他半导体材料构建异质结或 p-n 结,实现基于 Ga_2O_3 的自驱动日盲探测器。

2016 年,Chen 等^[145] 基于 $\beta\text{-Ga}_2\text{O}_3$ 纳米线阵列制备肖特基结自驱动日盲光电探测器。实验通过热氧化方法在蓝宝石衬底上合成 $\beta\text{-Ga}_2\text{O}_3$ 纳米线阵列,并在薄膜表面沉积 20 nm 厚的 Au 薄膜电极,底部为 Ga 欧姆接触,图 15(a) 给出了器件制备过程。在暗环境下,二极管表现出较好的整流特性,±15 V 时的整流比为 10^5 ,开启电压约为 10 V,反向 30 V 偏压下的漏电流低于~10 pA。此外,该器件具有明显的光伏效应,开路光电压和短路电流分别为 0.36 V 和 120 pA[图 15(b)]。在 0 V 和反向 10 V 偏压下,光响应截止波长约为 270 nm,器件对波长大于 310 nm 的光照几乎无响应[图 15(c)],上

升、下降时间为 $1 \mu\text{s}$ 和 $64 \mu\text{s}$,这在高速安全通信方面具有较大的应用潜力。

2017 年,Li 等^[147] 在 p 型 GaN 薄膜表面通过 PLD 技术在 750 °C 条件下沉积 $\beta\text{-Ga}_2\text{O}_3$ 薄膜,其中 GaN 薄膜 p 型 Mg 的掺杂浓度为 $6 \times 10^{16} \text{ cm}^{-3}$,载流子迁移率为 $10^2 \text{ cm}^2 \cdot \text{V}^{-1} \cdot \text{s}^{-1}$;他们分别在 GaN 和 $\beta\text{-Ga}_2\text{O}_3$ 薄膜表面通过直流溅射 Ag/In 电极制备日盲探测器。接近零偏压时,器件出现明显的光伏效应,在 254 nm($150 \mu\text{W}/\text{cm}^2$)光照下,开路电压和短路电流分别为 0.31 V 和 16.3 nA。随着所加偏压变大,氧空位释放的载流子数量增加,器件暗电流逐渐增加。在零偏压下,耗尽层的光生电子-空穴对被内建电场快速、有效分离并传输到相应电极且被收集,以产生光电流,通过掺杂调控材料的费米能级可使器件具有更大的内建电场,这对制备高性能自驱动日盲探测器具有重要意义。此外,该研究组还报道了基于 $\beta\text{-Ga}_2\text{O}_3$ 和 Ga 掺杂 ZnO(Ga : ZnO)的异质结器件。异质结在 3 V 和 -3 V 下的电流密度比值 $J_{(3 \text{ V})}/J_{(-3 \text{ V})}$ 超过 10^6 ,在零偏压下器件暗电流和光电流密度分别为 $0.15 \text{ nA}/\text{cm}^2$ 和 $38.3 \text{ nA}/\text{cm}^2$,开/关比约为 127^[222]。

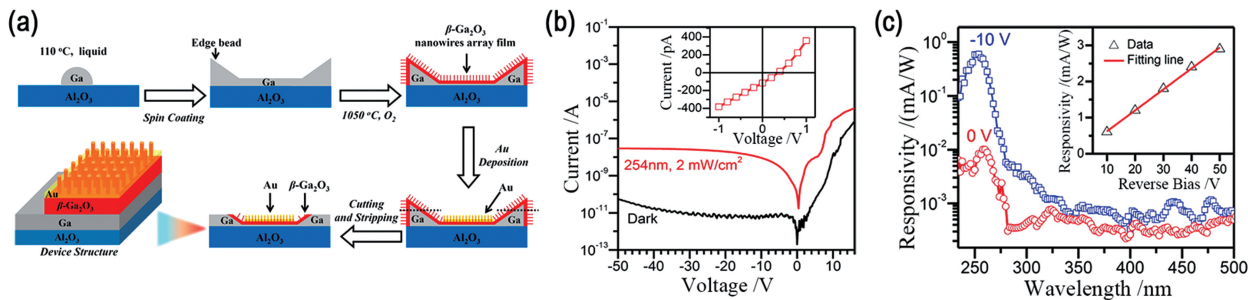


图 15 $\beta\text{-Ga}_2\text{O}_3$ 纳米线光电二极管的制备过程及其光电特性^[145]。(a) $\beta\text{-Ga}_2\text{O}_3$ 纳米线阵列薄膜及其垂直肖特基光电二极管的制备示意图;(b)器件在黑暗及 254 nm 光照下的 I-V 特性;(c)器件的光谱响应

Fig. 15 Fabrication process and photoelectric properties of $\beta\text{-Ga}_2\text{O}_3$ nanowires photodiode^[145]. (a) Schematic illustration of the fabrication of $\beta\text{-Ga}_2\text{O}_3$ nanowires array film and its vertical Schottky photodiode; (b) I-V characteristics of device in dark and under the illumination at 254 nm; (c) spectral response of the device

2017 年,Zhao 等^[223] 制备单根 ZnO- Ga_2O_3 异质结自驱动日盲探测器。在反向偏压、254 nm 光照条件下,异质结光电流超过暗电流两个数量级。此外,器件在 0 V 时的最大响应度位于 251 nm(9.7 mA/W),截止波长为 266 nm, $R_{251 \text{ nm}}/R_{400 \text{ nm}}$ 约为 6.9×10^2 ,器件对 266 nm 脉冲激光的上升、下降时间分别为 $100 \mu\text{s}$ 和 $900 \mu\text{s}$ 。2018 年,Arora 等^[224] 在 p 型 Si 衬底上通过射频磁控溅射生长 $\beta\text{-Ga}_2\text{O}_3$ 薄膜,沉积薄膜前首先在 700 °C 条件下溅射 $\sim 15 \text{ nm}$ 厚的晶种层,薄膜沉积完成后在 $\beta\text{-Ga}_2\text{O}_3$

薄膜表面镀 Cr/Au 电极(Cr 和 Au 电极的厚度分别为 50 nm 和 120 nm),制备 MSM 结构的日盲探测器。器件在 0 V 时的暗电流约为 1.43 pA,在 254 nm 光照下光电流增加到 5.1 nA,光暗电流比超过 10^3 ,同时具有较短的响应时间(上升、下降时间分别为 $32 \mu\text{s}$ 和 $78 \mu\text{s}$)。在外加偏压条件下(5 V),探测器对 250 nm 光照($44 \text{ nW}/\text{cm}^2$)的响应度为 96.13 A/W,EQE 为 $4.76 \times 10^4 \%$,器件对微弱信号具有较强的探测能力,该报道为开发用于探测微弱信号的 $\beta\text{-Ga}_2\text{O}_3$ 基自驱动日盲探测器提供

了思路。

2018 年, Chen 等^[148] 基于金刚石和 $\beta\text{-Ga}_2\text{O}_3$ 制备异质结日盲紫外探测器, 并将其应用于日盲成像。在零偏压下, 器件的最大响应度位于 244 nm, 由于金刚石对深紫外光的响应, 在 216 nm 位置同样出现光响应峰, 器件紫外-可见光抑制比 $R_{244\text{ nm}}/R_{400\text{ nm}}$ 为 135[图 16(a)], 暗电流密度 $J_d = 2.6 \times 10^{-9} \text{ A/cm}^2$ 。在零偏压、紫外“开”/“关”循环光照条件下, 器件表现出较好的稳定性和可重复性。最后, 将该器件用于日盲成像, 用空心“UV”图检测成像效果, 发现成像图形和原“UV”图较相似[图 16(b)], 成像图形具有良好的保真性。

2018 年, Guo 等^[3] 通过 Sn 掺杂调控 Ga_2O_3 ($\text{Sn} : \text{Ga}_2\text{O}_3$) 带隙, 并基于 p 型 GaN 制备 $\text{GaN}/\text{Sn} : \text{Ga}_2\text{O}_3$ p-n 结自驱动日盲探测器。器件在 0 V 时暗电流为 $9 \times 10^{-11} \text{ A}$, 光暗电流比为 6.1×10^4 , 随着光照强度的增加, 器件光电流明显增加, 在 254 nm 光照下 ($50 \mu\text{W/cm}^2$) 器件具有最大响应度 3.05 A/W。与该组之前报道中使用的纯 Ga_2O_3 相比^[147], 器件探测性能大幅度提升, $\text{GaN/Sn} : \text{Ga}_2\text{O}_3$

p-n 结势垒明显提高, 这归因于 Sn 掺杂使得 Ga_2O_3 费米能级更接近导带底, 从而使得 p-n 结内建电势变大, 光生载流子能更快速、有效分离。

众所周知, 二维材料应用于光电探测器时器件往往表现出较好的探测性能^[115, 190, 225-226]。2018 年, Zhuo 等^[151] 基于 MoS_2 和 $\beta\text{-Ga}_2\text{O}_3$ 制备异质结日盲探测器, MoS_2 和 $\beta\text{-Ga}_2\text{O}_3$ 表面镀 Au 和 Ti/Au 电极。0 V 时器件暗电流为 $2.1 \times 10^{-13} \text{ A}$, 在 254 nm 光照下器件光电流增加到 $2.8 \times 10^{-9} \text{ A}$ [图 16(c)], 光伏效应较明显。此外, 器件截止波长为 260 nm, $R_{245\text{ nm}}/R_{400\text{ nm}}$ 为 1.6×10^3 , 光电流明显依赖于光照强度且随着光强度的增加而增加[图 16(d)]。除此之外, 研究人员基于 $\alpha\text{-Ga}_2\text{O}_3$ 同样制备出了自驱动日盲探测器^[227]。实验采用 $\alpha\text{-Ga}_2\text{O}_3$ 纳米棒阵列和 Cu_2O 微米球制备 p-n 结并将其作为光电化学的工作电极, 用 Pt 作为对电极, 饱和甘汞作为参比电极, 制备了三电极光电化学型的光电探测器[图 16(e)]。与纯 $\alpha\text{-Ga}_2\text{O}_3$ 纳米棒阵列和 Cu_2O 微米球相比, $\alpha\text{-Ga}_2\text{O}_3/\text{Cu}_2\text{O}$ p-n 结具有更高的响应度和更大的光暗电流比[图 16(f)]。2019 年, Mitra

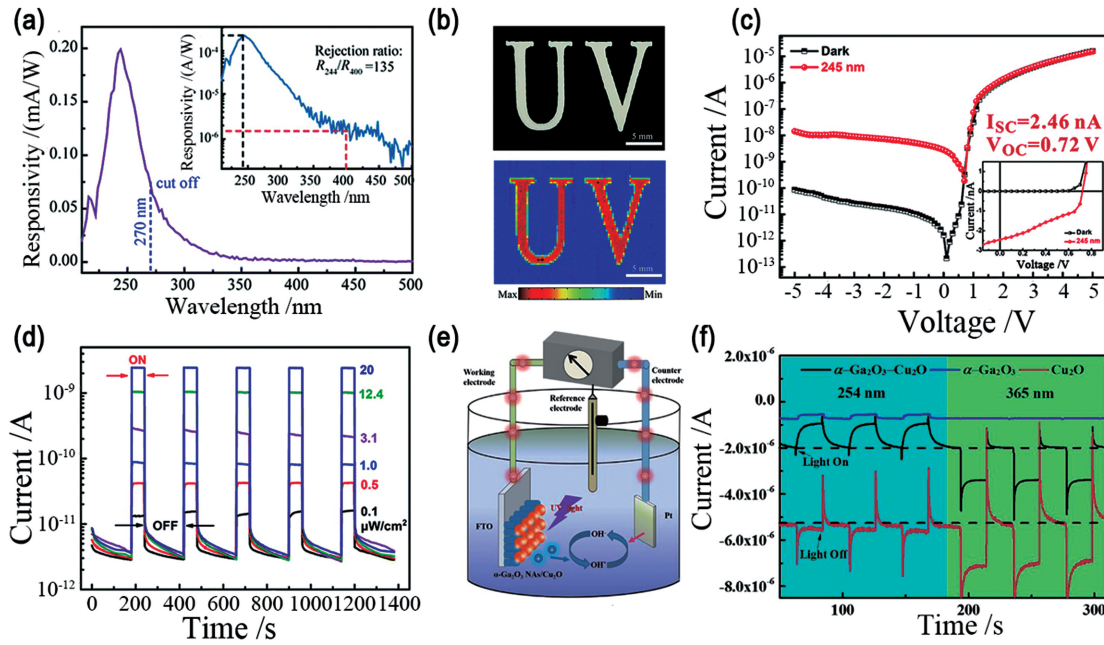


图 16 $\beta\text{-Ga}_2\text{O}_3$ 光电探测器的成像和光响应。(a) 光电探测器在 0 V 偏压下的光谱响应^[148]; (b) 黑纸上带有“UV”的图片及从成像系统中得到的图像^[148]; (c) $\text{MoS}_2/\beta\text{-Ga}_2\text{O}_3$ 异质结器件的 I - V 曲线^[151]; (d) 器件的时间响应谱^[151]; (e) 构建用于评估 $\alpha\text{-Ga}_2\text{O}_3/\text{Cu}_2\text{O}$ 光电探测器光响应行为的典型 PEC 系统^[227]; (f) 器件在零偏压下的瞬态响应电流^[227]

Fig. 16 Imaging and photoresponse of $\beta\text{-Ga}_2\text{O}_3$ photodetectors. (a) Spectral response of the diamond/ $\beta\text{-Ga}_2\text{O}_3$ photodetector at 0 V bias^[148]; (b) image of the object with letters “UV” on a black paper and the image obtained from the imaging system^[148]; (c) I - V curves of the $\text{MoS}_2/\beta\text{-Ga}_2\text{O}_3$ heterojunction device^[151]; (d) time-dependent photoresponse of the device^[151]; (e) typical PEC system built for evaluating the photoresponse behaviors of the $\alpha\text{-Ga}_2\text{O}_3/\text{Cu}_2\text{O}$ photodetector^[227]; (f) transient response current for the photodetector at zero bias^[227]

等^[228]制备非晶态 Ga_2O_3 核-壳纳米颗粒自驱动日盲探测器,其中核材料为富 Ga 态,壳材料为富 O 态,器件在零偏压下的光响应度为 15.3 mA/W ,探测度为 $0.63 \times 10^{11} \text{ Jones}$ 。

2020 年,Li 等^[229]通过 MOCVD 技术在蓝宝石衬底上沉积 $\beta\text{-}\text{Ga}_2\text{O}_3$ 薄膜,并通过旋涂法在 Ga_2O_3 表面制备 PEDOT : PSS 薄膜,最后通过在薄膜表面镀 Ti/Au 电极制备 PEDOT : PSS/ Ga_2O_3 有机-无机混合异质结自驱动日盲探测器。 Ga_2O_3 薄膜中较低的本征载流子浓度使得器件暗电流较低($-1 \text{ V}, 3.7 \text{ pA}$)^[223],在零偏压、 254 nm 光照下,器件光电流为 80 nA ,开路电压为 0.9 V ,探测度为 $9.2 \times 10^{12} \text{ Jones}$,光电流与光照强度几乎呈线性关

系,同时器件响应速度明显快于众多 Ga_2O_3 基光伏型探测器。此外,Wang 等^[230]基于聚苯胺(PANI)和 $\beta\text{-}\text{Ga}_2\text{O}_3$ 制备的 $\beta\text{-}\text{Ga}_2\text{O}_3/\text{PANI}$ 异质结日盲探测器的暗电流为 0.17 pA ,在 0 V 时最大光响应位于 246 nm ,截止波长为 272 nm ,如图 17(a)、(b)所示。Spiro-MeOTAD 由于性能优越而被广泛用于钙钛矿太阳能电池的空穴传输层^[231-232],在最近的报道中,Yan 等^[233]制备了 $\beta\text{-}\text{Ga}_2\text{O}_3/\text{Spiro-MeOTAD}$ p-n 异质结日盲紫外探测器,器件在零偏压下的暗电流为 $7.5 \times 10^{-14} \text{ A}$,光暗电流比($I_{\text{light}}/I_{\text{dark}}$)为 1.5×10^5 。此外,异质结光响应随入射光强度的增加而逐渐增加, $R_{250 \text{ nm}}/R_{400 \text{ nm}}$ 为 3.6×10^3 ,上升、下降时间分别为 $2.98 \mu\text{s}$ 和 $28.49 \mu\text{s}$ [图 17(c)、(d)]。

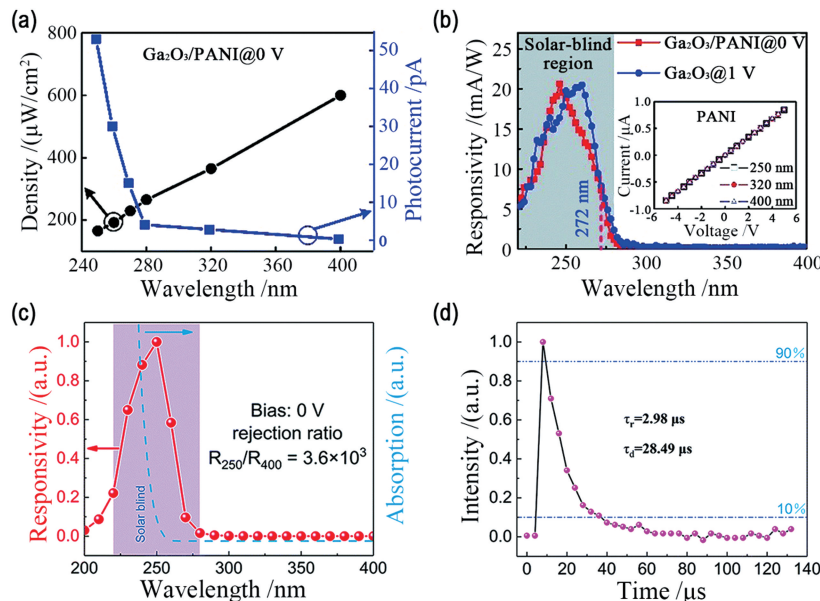


图 17 $\beta\text{-}\text{Ga}_2\text{O}_3$ 探测器的光谱响应和脉冲响应。(a)光电流及入射光功率密度与入射波长的函数关系^[230]; (b)0 V 时的 $\beta\text{-}\text{Ga}_2\text{O}_3/\text{PANI}$ 器件及 1 V 时作为参考的 $\beta\text{-}\text{Ga}_2\text{O}_3$ 探测器的光谱响应^[230]; (c)光电探测器的光谱响应及对应的吸收谱^[233]; (d)未加偏压时器件对 248 nm 脉冲激光的时间响应^[233]

Fig. 17 Spectral response and impulse response of $\beta\text{-}\text{Ga}_2\text{O}_3$ photodetector. (a) Photocurrent and power density as functions of excitation wavelength^[230]; (b) spectral response of reference $\beta\text{-}\text{Ga}_2\text{O}_3$ photodetector at 1 V bias and $\beta\text{-}\text{Ga}_2\text{O}_3/\text{PANI}$ at zero bias^[230]; (c) spectral responsivity and corresponding absorption spectrum of the photodetector^[233]; (d) time response of the photodetector for the 248 nm pulse laser without bias^[233]

6 结论与展望

Ga_2O_3 较大的禁带宽度($4.2 \sim 5.3 \text{ eV}$)几乎占据整个日盲波段,被认为是制备日盲紫外探测器的一种重要选择。本综述介绍了 Ga_2O_3 的晶体结构及基本特性,并简要综述了 Ga_2O_3 不同类型结构的材料合成研究进展。同时,按时间顺序介绍了基于 Ga_2O_3 纳米结构、单晶、薄膜三种形态的日盲紫外探测器及其异质结、自驱动器件的国内外研究进展。

在材料合成方面,随着国内外单晶制备技术越来越成熟,目前实际中已能够生长 Ga_2O_3 单晶,而通过 MOCVD、MBE、磁控溅射等技术沉积高质量大面积的 Ga_2O_3 薄膜的工艺路线已经成熟。从基于不同形态的 Ga_2O_3 日盲探测器来看,基于 Ga_2O_3 纳米线的日盲探测器表现出较高的响应度和外量子效率,最大光响应度超过 10^3 A/W ,外量子效率能达到 $10^5 \%$ 。 Ga_2O_3 单晶衬底及其剥离的单晶薄片基日盲探测器的光响应度高达 $10^3 \sim 10^5 \text{ A/W}$,外量子效

率超过 $10^6\%$ 。 Ga_2O_3 薄膜型器件的外量子效率大于 $10^5\%$ ，响应度超过 10^3 A/W ，同时器件暗电流能达到 pA 级别，且响应速度较快(μs 级)。 Ga_2O_3 基异质结(或p-n结)、肖特基结型探测器由于存在内部增益机制，其性能普遍高于光电导型器件。此外，目前的研究主要集中在非晶及 β 相 Ga_2O_3 ，针对 Ga_2O_3 其他相的器件的应用研究相对较少，但已报道的基于 Ga_2O_3 其他相(α, ϵ)的日盲探测器同样具有高探测性能。在未来的工作中，相信对于不同结构 Ga_2O_3 及其器件的研究将主要集中在以下方面：

1) 精确控制 Ga_2O_3 纳米材料的尺寸及形貌结构，采用掺杂等方式降低表面态并调控内部缺陷，此外，还应开发普遍适用的方法以提高具有良好排列和均匀分布的 Ga_2O_3 纳米材料的产量，这对于研制高性能器件至关重要。

2) 生长大直径、高质量的 Ga_2O_3 单晶衬底仍是一项重要挑战，应深入研究单晶生长中缺陷对晶体质量的影响，同时应该优化制备工艺，控制单晶中的杂质，这是生长高质量 Ga_2O_3 单晶的重要影响因素。

3) Ga_2O_3 材料的p型导电是目前面临的关键问题，可以尝试在其他相 Ga_2O_3 中进行非平衡掺杂。据报道， ϵ - Ga_2O_3 中的自发极化可能有助于降低受主电离能并促进p型导电，这对研究 Ga_2O_3 p型导电具有重要意义。

4) 目前 Ga_2O_3 基日盲探测器的研究主要集中在单个器件，在今后的工作中应发展相关的集成技术，解决器件的排列、组装等问题，研制具有功耗低、体积小、与CMOS读出电路兼容性好、集成度高等优点的焦平面日盲成像系统等大面积探测器件，开展微弱信号处理及成像增强技术的研究，并尝试将 Ga_2O_3 日盲探测器与天基紫外预警技术相结合。

相信经过研究人员的不断努力， Ga_2O_3 基日盲紫外探测器一定能够早日应用于国防军事及民用领域。

参 考 文 献

- [1] Razeghi M, Rogalski A. Semiconductor ultraviolet detectors[J]. Journal of Applied Physics, 1996, 79(10): 7433-7473.
- [2] Qin Y, Long S B, Dong H, et al. Review of deep ultraviolet photodetector based on gallium oxide[J]. Chinese Physics B, 2019, 28(1): 018501.
- [3] Guo D Y, Su Y L, Shi H Z, et al. Self-powered ultraviolet photodetector with superhigh photoresponsivity (3.05 A/W) based on the GaN/pn junction [J]. ACS Nano, 2018, 12(12): 12827-12835.
- [4] Li Y B, Tokizono T, Liao M Y, et al. Efficient assembly of bridged β - Ga_2O_3 nanowires for solar-blind photodetection [J]. Advanced Functional Materials, 2010, 20(22): 3972-3978.
- [5] Singh Pratiyush A, Krishnamoorthy S, Vishnu Solanke S, et al. High responsivity in molecular beam epitaxy grown β - Ga_2O_3 metal semiconductor metal solar blind deep-UV photodetector[J]. Applied Physics Letters, 2017, 110(22): 221107.
- [6] Chen M X, Zhao B, Hu G F, et al. Piezo-phototronic effect modulated deep UV photodetector based on $\text{ZnO-Ga}_2\text{O}_3$ heterojunction microwire[J]. Advanced Functional Materials, 2018, 28(14): 1706379.
- [7] Muñoz E, Monroy E, Pau J L, et al. III nitrides and UV detection [J]. Journal of Physics: Condensed Matter, 2001, 13(32): 7115-7137.
- [8] Razeghi M. Short-wavelength solar-blind detectors—status, prospects, and markets [J]. Proceedings of the IEEE, 2002, 90(6): 1006-1014.
- [9] Sang L W, Liao M Y, Sumiya M. A comprehensive review of semiconductor ultraviolet photodetectors: from thin film to one-dimensional nanostructures[J]. Sensors, 2013, 13(8): 10482-10518.
- [10] Chiou Y Z, Tang J J. GaN photodetectors with transparent indium tin oxide electrodes[J]. Japanese Journal of Applied Physics, 2004, 43(7A): 4146-4149.
- [11] Rathkanthiwar S, Kalra A, Solanke S V, et al. Gain mechanism and carrier transport in high responsivity AlGaN-based solar blind metal semiconductor metal photodetectors [J]. Journal of Applied Physics, 2017, 121(16): 164502.
- [12] Balakrishnan K, Bandoh A, Iwaya M, et al. Influence of high temperature in the growth of low dislocation content AlN bridge layers on patterned 6H-SiC substrates by metalorganic vapor phase epitaxy[J]. Japanese Journal of Applied Physics, 2007, 46(14): L307-L310.
- [13] Lin G T, Mo Z K, Weng Y, et al. Microstructure and optical properties of c-AlN/TiN/Si(100) heterostructure[J]. Acta Optica Sinica, 2019, 39(8): 0816003.
- [14] Yang W, Hullavarad S S, Nagaraj B, et al. Compositonally-tuned epitaxial cubic $\text{Mg}_x\text{Zn}_{1-x}\text{O}$ on Si(100) for deep ultraviolet photodetectors [J].

- Applied Physics Letters, 2003, 82(20): 3424-3426.
- [15] Chen X H, Ren F F, Gu S L, et al. Review of gallium-oxide-based solar-blind ultraviolet photodetectors[J]. Photonics Research, 2019, 7(4): 381-415.
- [16] Mahajan B K, Chen Y P, Noh J, et al. Electrothermal performance limit of β -Ga₂O₃ field-effect transistors[J]. Applied Physics Letters, 2019, 115(17): 173508.
- [17] Lu X, Zhou L D, Chen L, et al. Schottky X-ray detectors based on a bulk β -Ga₂O₃ substrate [J]. Applied Physics Letters, 2018, 112(10): 103502.
- [18] Suzuki R, Nakagomi S, Kokubun Y, et al. Enhancement of responsivity in solar-blind β -Ga₂O₃ photodiodes with a Au Schottky contact fabricated on single crystal substrates by annealing [J]. Applied Physics Letters, 2009, 94(22): 222102.
- [19] Roy R, Hill V G, Osborn E F. Polymorphism of Ga₂O₃ and the system Ga₂O₃-H₂O[J]. Journal of the American Chemical Society, 1952, 74(3): 719-722.
- [20] Schewski R, Wagner G, Baldini M, et al. Epitaxial stabilization of pseudomorphic α -Ga₂O₃ on sapphire (0001)[J]. Applied Physics Express, 2014, 8(1): 011101.
- [21] Qian H S, Gunawan P, Zhang Y X, et al. Template-free synthesis of highly uniform α -GaOOH spindles and conversion to α -Ga₂O₃ and β -Ga₂O₃[J]. Crystal Growth & Design, 2008, 8(4): 1282-1287.
- [22] Oshima Y, Villora E G, Shimamura K. Halide vapor phase epitaxy of twin-free α -Ga₂O₃ on sapphire (0001) substrates [J]. Applied Physics Express, 2015, 8(5): 055501.
- [23] Akaiwa K, Fujita S. Electrical conductive corundum-structured α -Ga₂O₃ thin films on sapphire with tin-doping grown by spray-assisted mist chemical vapor deposition[J]. Japanese Journal of Applied Physics, 2012, 51(7R): 070203.
- [24] Dong L P, Yu J G, Zhang Y M, et al. Elements (Si, Sn, and Mg) doped α -Ga₂O₃: first-principles investigations and predictions [J]. Computational Materials Science, 2019, 156: 273-279.
- [25] Morimoto S, Nishinaka H, Yoshimoto M. Growth and characterization of F-doped α -Ga₂O₃ thin films with low electrical resistivity[J]. Thin Solid Films, 2019, 682: 18-23.
- [26] Marezio M, Remeika J P. Bond lengths in the α -Ga₂O₃ structure and the high-pressure phase of Ga_{2-x}Fe_xO₃[J]. The Journal of Chemical Physics, 1967, 46(5): 1862-1865.
- [27] Shinohara D, Fujita S. Heteroepitaxy of corundum-structured α -Ga₂O₃ thin films on α -Al₂O₃ substrates by ultrasonic mist chemical vapor deposition [J]. Japanese Journal of Applied Physics, 2008, 47(9): 7311-7313.
- [28] Kaneko K, Nomura T, Fujita S. Corundum-structured α -phase Ga₂O₃-Cr₂O₃-Fe₂O₃ alloy system for novel functions [J]. Physica Status Solidi (c), 2010, 7(10): 2467-2470.
- [29] Playford H Y, Hannon A C, Barney E R, et al. Structures of uncharacterised polymorphs of gallium oxide from total neutron diffraction[J]. Chemistry, 2013, 19(8): 2803-2813.
- [30] Zinkevich M, Morales F M, Nitsche H, et al. Microstructural and thermodynamic study of γ -Ga₂O₃[J]. Zeitschrift Für Metallkunde, 2004, 95(9): 756-762.
- [31] Playford H Y, Hannon A C, Tucker M G, et al. Characterization of structural disorder in γ -Ga₂O₃[J]. The Journal of Physical Chemistry C, 2014, 118(29): 16188-16198.
- [32] Nakatani T, Watanabe T, Takahashi M, et al. Characterization of Gamma-Ga₂O₃-Al₂O₃ prepared by solvothermal method and its performance for methane-SCR of NO [J]. The Journal of Physical Chemistry A, 2009, 113(25): 7021-7029.
- [33] Watanabe T, Miki Y, Masuda T, et al. Performance of γ -Ga₂O₃-Al₂O₃ solid solutions prepared by spray pyrolysis for CH₄-SCR of NO[J]. Applied Catalysis A: General, 2011, 396(1/2): 140-147.
- [34] Kim J, Tahara D, Miura Y, et al. First-principle calculations of electronic structures and polar properties of (κ , ϵ)-Ga₂O₃[J]. Applied Physics Express, 2018, 11(6): 061101.
- [35] Oshima Y, Villora E G, Matsushita Y, et al. Epitaxial growth of phase-pure ϵ -Ga₂O₃ by halide vapor phase epitaxy[J]. Journal of Applied Physics, 2015, 118(8): 085301.
- [36] Cho S B, Mishra R. Epitaxial engineering of polar ϵ -Ga₂O₃ for tunable two-dimensional electron gas at the heterointerface[J]. Applied Physics Letters, 2018, 112(16): 162101.
- [37] Xia X C, Chen Y P, Feng Q J, et al. Hexagonal phase-pure wide band gap ϵ -Ga₂O₃ films grown on 6H-SiC substrates by metal organic chemical vapor deposition[J]. Applied Physics Letters, 2016, 108(20): 202103.
- [38] Tahara D, Nishinaka H, Morimoto S, et al. Stoichiometric control for heteroepitaxial growth of smooth ϵ -Ga₂O₃ thin films on c-plane AlN templates by mist chemical vapor deposition [J]. Japanese Journal of Applied Physics, 2017, 56(7): 078004.
- [39] Nishinaka H, Tahara D, Yoshimoto M. Heteroepitaxial

- growth of ϵ -Ga₂O₃ thin films on cubic (111) MgO and (111) yttria-stabilized zirconia substrates by mist chemical vapor deposition [J]. Japanese Journal of Applied Physics, 2016, 55(12): 1202BC.
- [40] Mezzadri F, Calestani G, Boschi F, et al. Crystal structure and ferroelectric properties of ϵ -Ga₂O₃ films grown on (0001)-sapphire[J]. Inorganic Chemistry, 2016, 55(22): 12079-12084.
- [41] Yoshioka S, Hayashi H, Kuwabara A, et al. Structures and energetics of Ga₂O₃ polymorphs[J]. Journal of Physics: Condensed Matter, 2007, 19(34): 346211.
- [42] Pearton S J, Yang J C, Cary P H, et al. A review of Ga₂O₃ materials, processing, and devices [J]. Applied Physics Reviews, 2018, 5(1): 011301.
- [43] Higashiwaki M, Sasaki K, Murakami H, et al. Recent progress in Ga₂O₃ power devices [J]. Semiconductor Science and Technology, 2016, 31(3): 034001.
- [44] Kananen B E, Halliburton L E, Stevens K T, et al. Gallium vacancies in β -Ga₂O₃ crystals[J]. Applied Physics Letters, 2017, 110(20): 202104.
- [45] Kananen B E, Halliburton L E, Scherrer E M, et al. Electron paramagnetic resonance study of neutral Mg acceptors in β -Ga₂O₃ crystals[J]. Applied Physics Letters, 2017, 111(7): 072102.
- [46] Bermudez V M. The structure of low-index surfaces of β -Ga₂O₃[J]. Chemical Physics, 2006, 323(2/3): 193-203.
- [47] Peelaers H, van de Walle C G. Brillouin zone and band structure of β -Ga₂O₃[J]. Physica Status Solidi (b), 2015, 252(4): 828-832.
- [48] Passlack M, Schubert E F, Hobson W S, et al. Ga₂O₃ films for electronic and optoelectronic applications[J]. Journal of Applied Physics, 1995, 77(2): 686-693.
- [49] Huang Y, Yue S L, Wang Z L, et al. Preparation and electrical properties of ultrafine Ga₂O₃ nanowires [J]. The Journal of Physical Chemistry B, 2006, 110(2): 796-800.
- [50] Varley J B, Weber J R, Janotti A, et al. Oxygen vacancies and donor impurities in β -Ga₂O₃ [J]. Applied Physics Letters, 2010, 97(14): 142106.
- [51] Hajnal Z, Miró J, Kiss G, et al. Role of oxygen vacancy defect states in the n-type conduction of β -Ga₂O₃[J]. Journal of Applied Physics, 1999, 86(7): 3792-3796.
- [52] Li Y, Yang C H, Wu L Y, et al. Electrical and optical properties of Si-doped Ga₂O₃ [J]. Modern Physics Letters B, 2017, 31(15): 1750172.
- [53] Villora E G, Shimamura K, Yoshikawa Y, et al. Electrical conductivity and carrier concentration control in β -Ga₂O₃ by Si doping[J]. Applied Physics Letters, 2008, 92(20): 202120.
- [54] Chikoidze E, von Bardeleben H J, Akaiwa K, et al. Electrical, optical, and magnetic properties of Sn doped α -Ga₂O₃ thin films[J]. Journal of Applied Physics, 2016, 120(2): 025109.
- [55] Higashiwaki M, Sasaki K, Kuramata A, et al. Gallium oxide (Ga₂O₃) metal-semiconductor field-effect transistors on single-crystal β -Ga₂O₃ (010) substrates[J]. Applied Physics Letters, 2012, 100(1): 013504.
- [56] Ahmadi E, Koksal O S, Kaun S W, et al. Ge doping of β -Ga₂O₃ films grown by plasma-assisted molecular beam epitaxy [J]. Applied Physics Express, 2017, 10(4): 041102.
- [57] Leedy K D, Chabak K D, Vasilyev V, et al. Highly conductive homoepitaxial Si-doped Ga₂O₃ films on (010) β -Ga₂O₃ by pulsed laser deposition [J]. Applied Physics Letters, 2017, 111(1): 012103.
- [58] Baldini M, Albrecht M, Fiedler A, et al. Semiconducting Sn-doped β -Ga₂O₃ homoepitaxial layers grown by metal organic vapour-phase epitaxy [J]. Journal of Materials Science, 2016, 51(7): 3650-3656.
- [59] Su Y L, Guo D Y, Ye J H, et al. Deep level acceptors of Zn-Mg divalent ions dopants in β -Ga₂O₃ for the difficulty to p-type conductivity[J]. Journal of Alloys and Compounds, 2019, 782: 299-303.
- [60] Qian Y P, Guo D Y, Chu X L, et al. Mg-doped p-type β -Ga₂O₃ thin film for solar-blind ultraviolet photodetector [J]. Materials Letters, 2017, 209: 558-561.
- [61] Wang X H, Zhang F B, Saito K, et al. Electrical properties and emission mechanisms of Zn-doped β -Ga₂O₃ films[J]. Journal of Physics and Chemistry of Solids, 2014, 75(11): 1201-1204.
- [62] Alema F, Hertog B, Ledyayev O, et al. Solar blind photodetector based on epitaxial zinc doped Ga₂O₃ thin film[J]. Physica Status Solidi (a), 2017, 214(5): 1600688.
- [63] Varley J B, Janotti A, Franchini C, et al. Role of self-trapping in luminescence and p-type conductivity of wide-band-gap oxides [J]. Physical Review B, 2012, 85(8): 081109.
- [64] Li L, Auer E, Liao M Y, et al. Deep-ultraviolet solar-blind photoconductivity of individual gallium oxide nanobelts[J]. Nanoscale, 2011, 3(3): 1120-1126.
- [65] Feng L G, Li Y F, Su X L, et al. Growth and characterization of spindle-like Ga₂O₃ nanocrystals by

- electrochemical reaction in hydrofluoric solution [J]. Applied Surface Science, 2016, 389: 205-210.
- [66] Wang T, Farvid S S, Abulikemu M, et al. Size-tunable phosphorescence in colloidal metastable γ - Ga_2O_3 nanocrystals [J]. Journal of the American Chemical Society, 2010, 132(27): 9250-9252.
- [67] Weng W Y, Hsueh T J, Chang S J, et al. A solar-blind β - Ga_2O_3 nanowire photodetector [J]. IEEE Photonics Technology Letters, 2010, 22(10): 709-711.
- [68] Dai Z R, Pan Z W, Wang Z L. Gallium oxide nanoribbons and nanosheets [J]. The Journal of Physical Chemistry B, 2002, 106(5): 902-904.
- [69] Hosein I D, Hegde M, Jones P D, et al. Evolution of the faceting, morphology and aspect ratio of gallium oxide nanowires grown by vapor-solid deposition [J]. Journal of Crystal Growth, 2014, 396: 24-32.
- [70] Cuong N D, Park Y W, Yoon S G. Microstructural and electrical properties of Ga_2O_3 nanowires grown at various temperatures by vapor-liquid-solid technique [J]. Sensors and Actuators B: Chemical, 2009, 140(1): 240-244.
- [71] Wu Y L, Chang S J, Weng W Y, et al. Ga_2O_3 nanowire photodetector prepared on SiO_2/Si template [J]. IEEE Sensors Journal, 2013, 13(6): 2368-2373.
- [72] Oh S, Kim J, Ren F, et al. Quasi-two-dimensional β -gallium oxide solar-blind photodetectors with ultrahigh responsivity [J]. Journal of Materials Chemistry C, 2016, 4(39): 9245-9250.
- [73] Oh S, Kim C K, Kim J. High responsivity β - Ga_2O_3 metal-semiconductor-metal solar-blind photodetectors with ultraviolet transparent graphene electrodes [J]. ACS Photonics, 2018, 5(3): 1123-1128.
- [74] Hwang W S, Verma A, Peelaers H, et al. High-voltage field effect transistors with wide-bandgap β - Ga_2O_3 nanomembranes [J]. Applied Physics Letters, 2014, 104(20): 203111.
- [75] Kwon Y, Lee G, Oh S, et al. Tuning the thickness of exfoliated quasi-two-dimensional β - Ga_2O_3 flakes by plasma etching [J]. Applied Physics Letters, 2017, 110(13): 131901.
- [76] Shin G, Kim H Y, Kim J. Deep-ultraviolet photodetector based on exfoliated n-type β - Ga_2O_3 nanobelt/p-Si substrate heterojunction [J]. Korean Journal of Chemical Engineering, 2018, 35(2): 574-578.
- [77] Yang G, Jang S, Ren F, et al. Influence of high-energy proton irradiation on β - Ga_2O_3 nanobelt field-effect transistors [J]. ACS Applied Materials & Interfaces, 2017, 9(46): 40471-40476.
- [78] Harwig T, Wubs G J, Dirksen G J. Electrical properties of β - Ga_2O_3 single crystals [J]. Solid State Communications, 1976, 18(9/10): 1223-1225.
- [79] Fleischer M, Meixner H. Electron mobility in single- and polycrystalline Ga_2O_3 [J]. Journal of Applied Physics, 1993, 74(1): 300-305.
- [80] Ueda N, Hosono H, Waseda R, et al. Synthesis and control of conductivity of ultraviolet transmitting β - Ga_2O_3 single crystals [J]. Applied Physics Letters, 1997, 70(26): 3561-3563.
- [81] Zhang J G, Li B, Xia C T, et al. Growth and spectral characterization of β - Ga_2O_3 single crystals [J]. Journal of Physics and Chemistry of Solids, 2006, 67(12): 2448-2451.
- [82] Ohba E, Kobayashi T, Kado M, et al. Defect characterization of β - Ga_2O_3 single crystals grown by vertical Bridgman method [J]. Japanese Journal of Applied Physics, 2016, 55(12): 1202BF.
- [83] Hoshikawa K, Ohba E, Kobayashi T, et al. Growth of β - Ga_2O_3 single crystals using vertical Bridgman method in ambient air [J]. Journal of Crystal Growth, 2016, 447: 36-41.
- [84] Aida H, Nishiguchi K, Takeda H, et al. Growth of β - Ga_2O_3 single crystals by the edge-defined, film fed growth method [J]. Japanese Journal of Applied Physics, 2008, 47(11): 8506-8509.
- [85] Mu W X, Jia Z T, Yin Y R, et al. High quality crystal growth and anisotropic physical characterization of β - Ga_2O_3 single crystals grown by EFG method [J]. Journal of Alloys and Compounds, 2017, 714: 453-458.
- [86] Galazka Z, Uecker R, Irmscher K, et al. Czochralski growth and characterization of β - Ga_2O_3 single crystals [J]. Crystal Research and Technology, 2010, 45(12): 1229-1236.
- [87] Tomm Y, Reiche P, Klimm D, et al. Czochralski grown Ga_2O_3 crystals [J]. Journal of Crystal Growth, 2000, 220(4): 510-514.
- [88] Chase A O. Growth of β - Ga_2O_3 by the verneuil technique [J]. Journal of the American Ceramic Society, 1964, 47(9): 470.
- [89] Villora E G, Shimamura K, Yoshikawa Y, et al. Large-size β - Ga_2O_3 single crystals and wafers [J]. Journal of Crystal Growth, 2004, 270(3/4): 420-426.
- [90] Galazka Z, Irmscher K, Uecker R, et al. On the bulk β - Ga_2O_3 single crystals grown by the Czochralski method [J]. Journal of Crystal Growth, 2014, 404: 184-191.
- [91] Kuramata A, Koshi K, Watanabe S, et al. High-quality β - Ga_2O_3 single crystals grown by edge-defined

- film-fed growth [J]. Japanese Journal of Applied Physics, 2016, 55(12): 1202A2.
- [92] Tang H L, He N T, Luo P, et al. Ultra-wide bandgap semiconductor β -Ga₂O₃ single crystal growth breaks through 2 inches [J]. Journal of Synthetic Crystals, 2017, 46(12): 2533-2534.
唐慧丽, 何诺天, 罗平, 等. 超宽禁带半导体 β -Ga₂O₃ 单晶生长突破 2 英寸 [J]. 人工晶体学报, 2017, 46(12): 2533-2534.
- [93] Zhang S N, Lian X Z, Ma Y C, et al. Growth and characterization of 2-inch high quality β -Ga₂O₃ single crystals grown by EFG method [J]. Journal of Semiconductors, 2018, 39(8): 083003.
- [94] Guo D Y, Wu Z P, Li P G, et al. Fabrication of β -Ga₂O₃ thin films and solar-blind photodetectors by laser MBE technology [J]. Optical Materials Express, 2014, 4(5): 1067-1076.
- [95] An Y H, Zhi Y S, Wu Z P, et al. Deep ultraviolet photodetectors based on p-Si/i-SiC/n-Ga₂O₃ heterojunction by inserting thin SiC barrier layer [J]. Applied Physics A, 2016, 122(12): 1036.
- [96] Liu X Z, Guo P, Sheng T, et al. β -Ga₂O₃ thin films on sapphire pre-seeded by homo-self-templated buffer layer for solar-blind UV photodetector [J]. Optical Materials, 2016, 51: 203-207.
- [97] Qu Y Y, Wu Z P, Ai M L, et al. Enhanced Ga₂O₃/SiC ultraviolet photodetector with graphene top electrodes [J]. Journal of Alloys and Compounds, 2016, 680: 247-251.
- [98] Ghose S, Rahman S, Hong L, et al. Growth and characterization of β -Ga₂O₃ thin films by molecular beam epitaxy for deep-UV photodetectors [J]. Journal of Applied Physics, 2017, 122(9): 095302.
- [99] Kalarickal N K, Xia Z B, McGlone J, et al. Mechanism of Si doping in plasma assisted MBE growth of β -Ga₂O₃ [J]. Applied Physics Letters, 2019, 115(15): 152106.
- [100] Chen Y P, Liang H W, Xia X C, et al. Effect of growth pressure on the characteristics of β -Ga₂O₃ films grown on GaAs (100) substrates by MOCVD method [J]. Applied Surface Science, 2015, 325: 258-261.
- [101] Du X J, Li Z, Luan C N, et al. Preparation and characterization of Sn-doped β -Ga₂O₃ homoepitaxial films by MOCVD [J]. Journal of Materials Science, 2015, 50(8): 3252-3257.
- [102] Feng X J, Li Z, Mi W, et al. Effect of annealing on the properties of Ga₂O₃: Mg films prepared on α -Al₂O₃ (0001) by MOCVD [J]. Vacuum, 2016, 124: 101-107.
- [103] Ma M H, Zhang D, Li Y Q, et al. High-performance solar blind ultraviolet photodetector based on single crystal orientation Mg-alloyed Ga₂O₃ film grown by a nonequilibrium MOCVD scheme [J]. ACS Applied Electronic Materials, 2019, 1(8): 1653-1659.
- [104] Hu D Q, Zhuang S W, Ma Z Z, et al. Study on the optical properties of β -Ga₂O₃ films grown by MOCVD [J]. Journal of Materials Science: Materials in Electronics, 2017, 28 (15): 10997-11001.
- [105] Anhar Uddin Bhuiyan A F M, Feng Z X, Johnson J M, et al. MOCVD epitaxy of β -(Al_xGa_{1-x})₂O₃ thin films on (010) Ga₂O₃ substrates and N-type doping [J]. Applied Physics Letters, 2019, 115 (12): 120602.
- [106] Orita M, Hiramatsu H, Ohta H, et al. Preparation of highly conductive, deep ultraviolet transparent β -Ga₂O₃ thin film at low deposition temperatures [J]. Thin Solid Films, 2002, 411(1): 134-139.
- [107] Ou S L, Wuu D S, Fu Y C, et al. Growth and etching characteristics of gallium oxide thin films by pulsed laser deposition [J]. Materials Chemistry and Physics, 2012, 133(2/3): 700-705.
- [108] Goyal A, Yadav B S, Thakur O P, et al. Effect of annealing on β -Ga₂O₃ film grown by pulsed laser deposition technique [J]. Journal of Alloys and Compounds, 2014, 583: 214-219.
- [109] Zhang F B, Saito K, Tanaka T, et al. Electrical properties of Si doped Ga₂O₃ films grown by pulsed laser deposition [J]. Journal of Materials Science: Materials in Electronics, 2015, 26(12): 9624-9629.
- [110] Lee S H, Kim S B, Moon Y J, et al. High-responsivity deep-ultraviolet-selective photodetectors using ultrathin gallium oxide films [J]. ACS Photonics, 2017, 4(11): 2937-2943.
- [111] Sheng J Z, Park E J, Shong B, et al. Atomic layer deposition of an indium gallium oxide thin film for thin-film transistor applications [J]. ACS Applied Materials & Interfaces, 2017, 9(28): 23934-23940.
- [112] Hao H, Chen X, Li Z C, et al. Remote plasma-enhanced atomic layer deposition of gallium oxide thin films with NH₃ plasma pretreatment [J]. Journal of Semiconductors, 2019, 40(1): 012806.
- [113] Sinha G, Adhikary K, Chaudhuri S. Sol-gel derived phase pure α -Ga₂O₃ nanocrystalline thin film and its optical properties [J]. Journal of Crystal Growth, 2005, 276(1/2): 204-207.
- [114] Kaya A, Mao H, Gao J Y, et al. An investigation of electrical and dielectric parameters of Sol-gel process enabled β -Ga₂O₃ as a gate dielectric material [J]. IEEE Transactions on Electron Devices, 2017,

- 64(5): 2047-2053.
- [115] Lin R C, Zheng W, Zhang D, et al. High-performance graphene/ β -Ga₂O₃ heterojunction deep-ultraviolet photodetector with hot-electron excited carrier multiplication[J]. ACS Applied Materials & Interfaces, 2018, 10(26): 22419-22426.
- [116] Shen H, Yin Y N, Tian K, et al. Growth and characterization of β -Ga₂O₃ thin films by Sol-gel method for fast-response solar-blind ultraviolet photodetectors [J]. Journal of Alloys and Compounds, 2018, 766: 601-608.
- [117] Li S, Guo D Y, Li P G, et al. Ultrasensitive, superhigh signal-to-noise ratio, self-powered solar-blind photodetector based on n-Ga₂O₃/p-CuSCN core-shell microwire heterojunction [J]. ACS Applied Materials & Interfaces, 2019, 11(38): 35105-35114.
- [118] Zhang Y J, Yan J L, Li Q S, et al. Optical and structural properties of Cu-doped β -Ga₂O₃ films[J]. Materials Science and Engineering: B, 2011, 176(11): 846-849.
- [119] Takakura K, Funasaki S, Tsunoda I, et al. Investigation of the Si doping effect in β -Ga₂O₃ films by co-sputtering of gallium oxide and Si[J]. Physica B: Condensed Matter, 2012, 407(15): 2900-2902.
- [120] An Y H, Chu X L, Huang Y Q, et al. Au plasmon enhanced high performance β -Ga₂O₃ solar-blind photo-detector [J]. Progress in Natural Science: Materials International, 2016, 26(1): 65-68.
- [121] Guo D Y, Liu H, Li P G, et al. Zero-power-consumption solar-blind photodetector based on β -Ga₂O₃/NSTO heterojunction [J]. ACS Applied Materials & Interfaces, 2017, 9(2): 1619-1628.
- [122] Guo D Y, Qin X Y, Lv M, et al. Decrease of oxygen vacancy by Zn-doped for improving solar-blind photoelectric performance in β -Ga₂O₃ thin films[J]. Electronic Materials Letters, 2017, 13(6): 483-488.
- [123] Lee S Y, Kang H C. Sn-doped β -Ga₂O₃ nanowires deposited by radio frequency powder sputtering[J]. Japanese Journal of Applied Physics, 2018, 57(1S): 01AE02.
- [124] Li M Q, Yang N, Wang G G, et al. Highly preferred orientation of Ga₂O₃ films sputtered on SiC substrates for deep UV photodetector application[J]. Applied Surface Science, 2019, 471: 694-702.
- [125] Xiu X Q, Zhang L Y, Li Y W, et al. Application of halide vapor phase epitaxy for the growth of ultra-wide band gap Ga₂O₃ [J]. Journal of Semiconductors, 2019, 40(1): 011805.
- [126] Nomura K, Goto K, Togashi R, et al. Thermodynamic study of β -Ga₂O₃ growth by halide vapor phase epitaxy[J]. Journal of Crystal Growth, 2014, 405: 19-22.
- [127] Oshima Y, Villora E G, Shimamura K. Quasi-heteroepitaxial growth of β -Ga₂O₃ on off-angled sapphire (0 0 0 1) substrates by halide vapor phase epitaxy[J]. Journal of Crystal Growth, 2015, 410: 53-58.
- [128] Polyakov A Y, Lee I H, Smirnov N B, et al. Defects at the surface of β -Ga₂O₃ produced by Ar plasma exposure[J]. APL Materials, 2019, 7(6): 061102.
- [129] Leach J H, Udwyar K, Rumsey J, et al. Halide vapor phase epitaxial growth of β -Ga₂O₃ and α -Ga₂O₃ films [J]. APL Materials, 2019, 7(2): 022504.
- [130] Zhang Y N, Zhang J C, Feng Z Q, et al. Impact of implanted edge termination on vertical β -Ga₂O₃ Schottky barrier diodes under OFF-state stressing [J]. IEEE Transactions on Electron Devices, 2020, 67(10): 3948-3953.
- [131] Sasaki K, Kuramata A, Masui T, et al. Device-quality β -Ga₂O₃ epitaxial films fabricated by ozone molecular beam epitaxy [J]. Applied Physics Express, 2012, 5(3): 035502.
- [132] Feng Z X, Bhuiyan A F M A U, Karim M R, et al. MOCVD homoepitaxy of Si-doped (010) β -Ga₂O₃ thin films with superior transport properties [J]. Applied Physics Letters, 2019, 114(25): 250601.
- [133] Ma N, Tanen N, Verma A, et al. Intrinsic electron mobility limits in β -Ga₂O₃ [J]. Applied Physics Letters, 2016, 109(21): 212101.
- [134] Miller R, Alema F, Osinsky A. Epitaxial β -Ga₂O₃ and β -(Al_xGa_{1-x})₂O₃/ β -Ga₂O₃ heterostructures growth for power electronics[J]. IEEE Transactions on Semiconductor Manufacturing, 2018, 31(4): 467-474.
- [135] Qiao G, Cai Q, Ma T C, et al. Nanoplasmonically enhanced high-performance metastable phase α -Ga₂O₃ solar-blind photodetectors[J]. ACS Applied Materials & Interfaces, 2019, 11(43): 40283-40289.
- [136] Qin Y, Li L H, Zhao X L, et al. Metal-semiconductor-metal ϵ -Ga₂O₃ solar-blind photodetectors with a record-high responsivity rejection ratio and their gain mechanism[J]. ACS Photonics, 2020, 7(3): 812-820.
- [137] Peng Y K, Zhang Y, Chen Z W, et al. Arrays of solar-blind ultraviolet photodetector based on β -Ga₂O₃ epitaxial thin films [J]. IEEE Photonics

- Technology Letters, 2018, 30(11): 993-996.
- [138] Chen Y C, Lu Y J, Liao M Y, et al. 3D solar-blind Ga_2O_3 photodetector array realized via origami method[J]. Advanced Functional Materials, 2019, 29(50): 1906040.
- [139] Cui S J, Mei Z X, Zhang Y H, et al. Room-temperature fabricated amorphous Ga_2O_3 high-response-speed solar-blind photodetector on rigid and flexible substrates [J]. Advanced Optical Materials, 2017, 5(19): 1700454.
- [140] Xie C, Lu X T, Liang Y, et al. Patterned growth of $\beta\text{-}\text{Ga}_2\text{O}_3$ thin films for solar-blind deep-ultraviolet photodetectors array and optical imaging application [J]. Journal of Materials Science & Technology, 2021, 72: 189-196.
- [141] Lai J Y, Hasan M N, Swinnich E, et al. Flexible crystalline $\beta\text{-}\text{Ga}_2\text{O}_3$ solar-blind photodetectors [J]. Journal of Materials Chemistry C, 2020, 8 (42): 14732-14739.
- [142] Oshima T, Okuno T, Arai N, et al. Vertical-solar-blind deep-ultraviolet Schottky photodetectors based on $\beta\text{-}\text{Ga}_2\text{O}_3$ Substrates [J]. Applied Physics Express, 2008, 1(1): 011202.
- [143] Pratiyush A S, Xia Z B, Kumar S, et al. MBE-grown $\beta\text{-}\text{Ga}_2\text{O}_3$ -based Schottky UV-C photodetectors with rectification ratio $\sim 10^7$ [J]. IEEE Photonics Technology Letters, 2018, 30(23): 2025-2028.
- [144] Liu Z, Wang X, Liu Y Y, et al. A high-performance ultraviolet solar-blind photodetector based on a $\beta\text{-}\text{Ga}_2\text{O}_3$ Schottky photodiode [J]. Journal of Materials Chemistry C, 2019, 7 (44): 13920-13929.
- [145] Chen X, Liu K W, Zhang Z Z, et al. Self-powered solar-blind photodetector with fast response based on Au/ $\beta\text{-}\text{Ga}_2\text{O}_3$ nanowires array film Schottky junction[J]. ACS Applied Materials & Interfaces, 2016, 8(6): 4185-4191.
- [146] Kokubun Y, Kubo S, Nakagomi S. All-oxide p-n heterojunction diodes comprising p-type NiO and n-type $\beta\text{-}\text{Ga}_2\text{O}_3$ [J]. Applied Physics Express, 2016, 9(9): 091101.
- [147] Li P G, Shi H Z, Chen K, et al. Construction of GaN/ Ga_2O_3 p-n junction for an extremely high responsivity self-powered UV photodetector [J]. Journal of Materials Chemistry C, 2017, 5 (40): 10562-10570.
- [148] Chen Y C, Lu Y J, Lin C N, et al. Self-powered diamond/ $\beta\text{-}\text{Ga}_2\text{O}_3$ photodetectors for solar-blind imaging [J]. Journal of Materials Chemistry C, 2018, 6(21): 5727-5732.
- [149] Nakagomi S, Sakai T, Kikuchi K, et al. $\beta\text{-}\text{Ga}_2\text{O}_3$ /p-type 4H-SiC heterojunction diodes and applications to deep-UV photodiodes [J]. Physica Status Solidi (a), 2019, 216(5): 1700796.
- [150] Zhao B, Wang F, Chen H Y, et al. Solar-blind avalanche photodetector based on single $\text{ZnO}\text{-}\text{Ga}_2\text{O}_3$ core-shell microwire [J]. Nano Letters, 2015, 15 (6): 3988-3993.
- [151] Zhuo R R, Wu D, Wang Y G, et al. A self-powered solar-blind photodetector based on a MoS_2 / $\beta\text{-}\text{Ga}_2\text{O}_3$ heterojunction [J]. Journal of Materials Chemistry C, 2018, 6(41): 10982-10986.
- [152] Feng P, Zhang J Y, Li Q H, et al. Individual $\beta\text{-}\text{Ga}_2\text{O}_3$ nanowires as solar-blind photodetectors [J]. Applied Physics Letters, 2006, 88(15): 153107.
- [153] Zou R, Zhang Z, Liu Q, et al. High detectivity solar-blind high-temperature deep-ultraviolet photodetector based on multi-layered (100) facet-oriented $\beta\text{-}\text{Ga}_2\text{O}_3$ nanobelts [J]. Small, 2014, 10 (9): 1848-1856.
- [154] Wang S L, Sun H L, Wang Z, et al. In situ synthesis of monoclinic $\beta\text{-}\text{Ga}_2\text{O}_3$ nanowires on flexible substrate and solar-blind photodetector [J]. Journal of Alloys and Compounds, 2019, 787: 133-139.
- [155] Xie C, Lu X T, Ma M R, et al. Catalyst-free vapor-solid deposition growth of $\beta\text{-}\text{Ga}_2\text{O}_3$ nanowires for DUV photodetector and image sensor application [J]. Advanced Optical Materials, 2019, 7 (24): 1901257.
- [156] Yang C, Liang H W, Zhang Z Z, et al. Self-powered SBD solar-blind photodetector fabricated on the single crystal of $\beta\text{-}\text{Ga}_2\text{O}_3$ [J]. RSC Advances, 2018, 8(12): 6341-6345.
- [157] Hu Z Y, Nomoto K, Li W S, et al. Breakdown mechanism in $1\text{ kA}/\text{cm}^2$ and 960 V E-mode $\beta\text{-}\text{Ga}_2\text{O}_3$ vertical transistors [J]. Applied Physics Letters, 2018, 113(12): 122103.
- [158] Lv Y, Zhou X Y, Long S B, et al. Source-field-plated $\beta\text{-}\text{Ga}_2\text{O}_3$ MOSFET with record power figure of merit of $50.4\text{ MW}/\text{cm}^2$ [J]. IEEE Electron Device Letters, 2019, 40(1): 83-86.
- [159] Zeng K, Vaidya A, Singisetti U. 1. 85 kV breakdown voltage in lateral field-plated Ga_2O_3 MOSFETs [J]. IEEE Electron Device Letters, 2018, 39(9): 1385-1388.
- [160] Mun J K, Cho K, Chang W, et al. Editors' choice — 2.32 kV breakdown voltage lateral $\beta\text{-}\text{Ga}_2\text{O}_3$ MOSFETs with source-connected field plate [J]. ECS Journal of Solid State Science and Technology, 2019, 8(7): Q3079-Q3082.

- [161] Sharma S, Zeng K, Saha S, et al. Field-plated lateral Ga_2O_3 MOSFETs with polymer passivation and 8.03 kV breakdown voltage[J]. IEEE Electron Device Letters, 2020, 41(6): 836-839.
- [162] Oshima T, Okuno T, Arai N, et al. Flame detection by a $\beta\text{-}\text{Ga}_2\text{O}_3$ -based sensor[J]. Japanese Journal of Applied Physics, 2009, 48(1): 011605.
- [163] Mu W X, Jia Z T, Yin Y R, et al. One-step exfoliation of ultra-smooth $\beta\text{-}\text{Ga}_2\text{O}_3$ wafers from bulk crystal for photodetectors[J]. CrystEngComm, 2017, 19(34): 5122-5127.
- [164] Liu Y X, Du L L, Liang G D, et al. Ga_2O_3 field-effect-transistor-based solar-blind photodetector with fast response and high photo-to-dark current ratio[J]. IEEE Electron Device Letters, 2018, 39(11): 1696-1699.
- [165] Lee S Y, Kim D H, Chong E, et al. Effect of channel thickness on density of states in amorphous InGaZnO thin film transistor[J]. Applied Physics Letters, 2011, 98(12): 122105.
- [166] Chen X H, Mu W X, Xu Y, et al. Highly narrow-band polarization-sensitive solar-blind photodetectors based on $\beta\text{-}\text{Ga}_2\text{O}_3$ single crystals[J]. ACS Applied Materials & Interfaces, 2019, 11(7): 7131-7137.
- [167] Weng W Y, Hsueh T J, Chang S J, et al. A $\beta\text{-}\text{Ga}_2\text{O}_3$ solar-blind photodetector prepared by furnace oxidation of GaN thin film[J]. IEEE Sensors Journal, 2011, 11(4): 999-1003.
- [168] Suzuki R, Nakagomi S, Kokubun Y. Solar-blind photodiodes composed of a Au Schottky contact and a $\beta\text{-}\text{Ga}_2\text{O}_3$ single crystal with a high resistivity cap layer[J]. Applied Physics Letters, 2011, 98(13): 131114.
- [169] Hu G C, Shan C X, Zhang N, et al. High gain Ga_2O_3 solar-blind photodetectors realized via a carrier multiplication process[J]. Optics Express, 2015, 23(10): 13554-13561.
- [170] Suzuki N, Ohira S, Tanaka M, et al. Fabrication and characterization of transparent conductive Sn-doped $\beta\text{-}\text{Ga}_2\text{O}_3$ single crystal [J]. Physica Status Solidi (c), 2007, 4(7): 2310-2313.
- [171] Wu Z P, Bai G X, Qu Y Y, et al. Deep ultraviolet photoconductive and near-infrared luminescence properties of Er^{3+} -doped $\beta\text{-}\text{Ga}_2\text{O}_3$ thin films[J]. Applied Physics Letters, 2016, 108(21): 211903.
- [172] Zhao X L, Zhi Y S, Cui W, et al. Characterization of hexagonal $\epsilon\text{-}\text{Ga}_{1.8}\text{Sn}_{0.2}\text{O}_3$ thin films for solar-blind ultraviolet applications[J]. Optical Materials, 2016, 62: 651-654.
- [173] Zhao X L, Wu Z P, Zhi Y S, et al. Improvement for the performance of solar-blind photodetector based on $\beta\text{-}\text{Ga}_2\text{O}_3$ thin films by doping Zn[J]. Journal of Physics D: Applied Physics, 2017, 50(8): 085102.
- [174] Li W H, Zhao X L, Zhi Y S, et al. Fabrication of cerium-doped $\beta\text{-}\text{Ga}_2\text{O}_3$ epitaxial thin films and deep ultraviolet photodetectors[J]. Applied Optics, 2018, 57(3): 538-543.
- [175] Lovejoy T C, Chen R Y, Zheng X, et al. Band bending and surface defects in $\beta\text{-}\text{Ga}_2\text{O}_3$ [J]. Applied Physics Letters, 2012, 100(18): 181602.
- [176] Huang L, Feng Q, Han G Q, et al. Comparison study of $\beta\text{-}\text{Ga}_2\text{O}_3$ photodetectors grown on sapphire at different oxygen pressures[J]. IEEE Photonics Journal, 2017, 9(4): 6803708.
- [177] Armstrong A M, Crawford M H, Jayawardena A, et al. Role of self-trapped holes in the photoconductive gain of β -gallium oxide Schottky diodes[J]. Journal of Applied Physics, 2016, 119(10): 103102.
- [178] Qian L X, Wu Z H, Zhang Y Y, et al. Ultrahigh-responsivity, rapid-recovery, solar-blind photodetector based on highly nonstoichiometric amorphous gallium oxide[J]. ACS Photonics, 2017, 4(9): 2203-2211.
- [179] Huang H L, Xie Y N, Zhang Z F, et al. Growth and fabrication of sputtered TiO_2 based ultraviolet detectors[J]. Applied Surface Science, 2014, 293: 248-254.
- [180] Carrano J C, Li T, Grudowski P A, et al. Comprehensive characterization of metal-semiconductor-metal ultraviolet photodetectors fabricated on single-crystal GaN[J]. Journal of Applied Physics, 1998, 83(11): 6148-6160.
- [181] Li H J, Zhang Y. Transmission spectrum of multilayer AlGaN thin film on sapphire substrate[J]. Acta Optica Sinica, 2020, 40(19): 1931002. 李浩杰, 张燕. 蓝宝石衬底多层 AlGaN 薄膜透射谱研究[J]. 光学学报, 2020, 40(19): 1931002.
- [182] Xu Y, An Z Y, Zhang L X, et al. Solar blind deep ultraviolet $\beta\text{-}\text{Ga}_2\text{O}_3$ photodetectors grown on sapphire by the Mist-CVD method[J]. Optical Materials Express, 2018, 8(9): 2941-2947.
- [183] Guo D Y, Wu Z P, An Y H, et al. Oxygen vacancy tuned Ohmic-Schottky conversion for enhanced performance in $\beta\text{-}\text{Ga}_2\text{O}_3$ solar-blind ultraviolet photodetectors[J]. Applied Physics Letters, 2014, 105(2): 023507.
- [184] Qiao B S, Zhang Z Z, Xie X H, et al. Avalanche gain in metal-semiconductor-metal Ga_2O_3 solar-blind photodiodes[J]. The Journal of Physical Chemistry C, 2019, 123(30): 18516-18520.

- [185] Han Z Y, Liang H L, Huo W X, et al. Boosted UV photodetection performance in chemically etched amorphous Ga_2O_3 thin-film transistors [J]. Advanced Optical Materials, 2020, 8(8): 1901833.
- [186] Lu H L, Zhou X L, Liang T, et al. Oxide thin-film transistors with IMO and IGZO stacked active layers for UV detection[J]. IEEE Journal of the Electron Devices Society, 2017, 5(6): 504-508.
- [187] Janotti A, van de Walle C G. Oxygen vacancies in ZnO [J]. Applied Physics Letters, 2005, 87(12): 122102.
- [188] Bae H S, Yoon M H, Kim J H, et al. Photodetecting properties of ZnO -based thin-film transistors[J]. Applied Physics Letters, 2003, 83(25): 5313-5315.
- [189] Xu Y, Chen X H, Zhou D, et al. Carrier transport and gain mechanisms in $\beta\text{-}\text{Ga}_2\text{O}_3$ -based metal-semiconductor-metal solar-blind Schottky photodetectors[J]. IEEE Transactions on Electron Devices, 2019, 66(5): 2276-2281.
- [190] Yu Y F, Ni Z H. Photodetection based on surface plasmon-induced hot electrons [J]. Laser & Optoelectronics Progress, 2019, 56(20): 202403. 于远方, 倪振华. 表面等离激元热电子光电探测[J]. 激光与光电子学进展, 2019, 56(20): 202403.
- [191] Guo D, Li P, Wu Z, et al. Inhibition of unintentional extra carriers by Mn valence change for high insulating devices[J]. Scientific Reports, 2016, 6: 24190.
- [192] Qian L X, Wang Y, Wu Z H, et al. $\beta\text{-}\text{Ga}_2\text{O}_3$ solar-blind deep-ultraviolet photodetector based on annealed sapphire substrate [J]. Vacuum, 2017, 140: 106-110.
- [193] Qian L X, Zhang H F, Lai P T, et al. High-sensitivity $\beta\text{-}\text{Ga}_2\text{O}_3$ solar-blind photodetector on high-temperature pretreated c-plane sapphire substrate[J]. Optical Materials Express, 2017, 7(10): 3643-3653.
- [194] Pratiyush A S, Krishnamoorthy S, Kumar S, et al. Demonstration of zero bias responsivity in MBE grown $\beta\text{-}\text{Ga}_2\text{O}_3$ lateral deep-UV photodetector[J]. Japanese Journal of Applied Physics, 2018, 57(6): 060313.
- [195] Qian L X, Liu H Y, Zhang H F, et al. Simultaneously improved sensitivity and response speed of $\beta\text{-}\text{Ga}_2\text{O}_3$ solar-blind photodetector via localized tuning of oxygen deficiency[J]. Applied Physics Letters, 2019, 114(11): 113506.
- [196] Han S, Huang X L, Fang M Z, et al. High-performance UV detectors based on room-temperature deposited amorphous Ga_2O_3 thin films by RF magnetron sputtering [J]. Journal of Materials Chemistry C, 2019, 7(38): 11834-11844.
- [197] Zhang Y F, Chen X H, Xu Y, et al. Transition of photoconductive and photovoltaic operation modes in amorphous Ga_2O_3 -based solar-blind detectors tuned by oxygen vacancies[J]. Chinese Physics B, 2019, 28(2): 028501.
- [198] Kalra A, Vura S, Rathkanthiwar S, et al. Demonstration of high-responsivity epitaxial $\beta\text{-}\text{Ga}_2\text{O}_3/\text{GaN}$ metal-heterojunction-metal broadband UV-A/UV-C detector [J]. Applied Physics Express, 2018, 11(6): 064101.
- [199] Chen X H, Han S, Lu Y M, et al. High signal/noise ratio and high-speed deep UV detector on $\beta\text{-}\text{Ga}_2\text{O}_3$ thin film composed of both (400) and (2 $\bar{1}$ 01) orientation $\beta\text{-}\text{Ga}_2\text{O}_3$ deposited by the PLD method [J]. Journal of Alloys and Compounds, 2018, 747: 869-878.
- [200] Li K H, Alfaraj N, Kang C H, et al. Deep-ultraviolet photodetection using single-crystalline $\beta\text{-}\text{Ga}_2\text{O}_3/\text{NiO}$ heterojunctions [J]. ACS Applied Materials & Interfaces, 2019, 11(38): 35095-35104.
- [201] Zhang D, Zheng W, Lin R C, et al. High quality $\beta\text{-}\text{Ga}_2\text{O}_3$ film grown with N_2O for high sensitivity solar-blind-ultraviolet photodetector with fast response speed [J]. Journal of Alloys and Compounds, 2018, 735: 150-154.
- [202] Li Y Q, Zhang D, Lin R C, et al. Graphene interdigital electrodes for improving sensitivity in a $\text{Ga}_2\text{O}_3 : \text{Zn}$ deep-ultraviolet photoconductive detector[J]. ACS Applied Materials & Interfaces, 2019, 11(1): 1013-1020.
- [203] Liu Z, Li S, Yan Z Y, et al. Construction of a $\beta\text{-}\text{Ga}_2\text{O}_3$ -based metal-oxide-semiconductor-structured photodiode for high-performance dual-mode solar-blind detector applications[J]. Journal of Materials Chemistry C, 2020, 8(15): 5071-5081.
- [204] Lee S H, Lee K M, Kim Y B, et al. Sub-microsecond response time deep-ultraviolet photodetectors using $\alpha\text{-}\text{Ga}_2\text{O}_3$ thin films grown via low-temperature atomic layer deposition[J]. Journal of Alloys and Compounds, 2019, 780: 400-407.
- [205] Moloney J, Tesh O, Singh M, et al. Atomic layer deposited $\alpha\text{-}\text{Ga}_2\text{O}_3$ solar-blind photodetectors [J]. Journal of Physics D: Applied Physics, 2019, 52(47): 475101.
- [206] Zhou C Q, Liu K W, Chen X, et al. Performance improvement of amorphous Ga_2O_3 ultraviolet photodetector by annealing under oxygen atmosphere[J]. Journal of Alloys and Compounds,

- 2020, 840: 155585.
- [207] Huang Z D, Weng W Y, Chang S J, et al. $\text{Ga}_2\text{O}_3/\text{AlGaN}/\text{GaN}$ heterostructure ultraviolet three-band photodetector[J]. IEEE Sensors Journal, 2013, 13(9): 3462-3467.
- [208] Nakagomi S, Sato T A, Takahashi Y, et al. Deep ultraviolet photodiodes based on the $\beta\text{-}\text{Ga}_2\text{O}_3/\text{GaN}$ heterojunction [J]. Sensors and Actuators A: Physical, 2015, 232: 208-213.
- [209] Guo X C, Hao N H, Guo D Y, et al. $\beta\text{-}\text{Ga}_2\text{O}_3/\text{p-Si}$ heterojunction solar-blind ultraviolet photodetector with enhanced photoelectric responsivity[J]. Journal of Alloys and Compounds, 2016, 660: 136-140.
- [210] Mahmoud W E. Solar blind avalanche photodetector based on the cation exchange growth of $\beta\text{-}\text{Ga}_2\text{O}_3/\text{SnO}_2$ bilayer heterostructure thin film [J]. Solar Energy Materials and Solar Cells, 2016, 152: 65-72.
- [211] Kong W Y, Wu G A, Wang K Y, et al. Graphene- $\beta\text{-}\text{Ga}_2\text{O}_3$ heterojunction for highly sensitive deep UV photodetector application[J]. Advanced Materials, 2016, 28(48): 10725-10731.
- [212] Chen X H, Xu Y, Zhou D, et al. Solar-blind photodetector with high avalanche gains and bias-tunable detecting functionality based on metastable phase $\alpha\text{-}\text{Ga}_2\text{O}_3/\text{ZnO}$ isotype heterostructures [J]. ACS Applied Materials & Interfaces, 2017, 9(42): 36997-37005.
- [213] Yu J, Shan C X, Huang X M, et al. ZnO-based ultraviolet avalanche photodetectors[J]. Journal of Physics D: Applied Physics, 2013, 46(30): 305105.
- [214] Wang Y H, Cui W J, Yu J, et al. One-step growth of amorphous/crystalline Ga_2O_3 phase junctions for high-performance solar-blind photodetection [J]. ACS Applied Materials & Interfaces, 2019, 11(49): 45922-45929.
- [215] Zhu T, Su J, Alvarez J, et al. Response enhancement of self-powered visible-blind UV photodetectors by nanostructured heterointerface engineering [J]. Advanced Functional Materials, 2019, 29(38): 1903981.
- [216] Zhang Y, Zhao X Y, Chen J X, et al. Self-polarized BaTiO_3 for greatly enhanced performance of ZnO UV photodetector by regulating the distribution of electron concentration [J]. Advanced Functional Materials, 2020, 30(5): 1907650.
- [217] Ouyang B S, Zhao H Q, Wang Z L, et al. Dual-polarity response in self-powered ZnO NWs/ Sb_2Se_3 film heterojunction photodetector array for optical communication [J]. Nano Energy, 2020, 68: 104312.
- [218] Hatch S M, Briscoe J, Dunn S. A self-powered ZnO-nanorod/CuSCN UV photodetector exhibiting rapid response[J]. Advanced Materials, 2013, 25(6): 867-871.
- [219] Leung S F, Ho K T, Kung P K, et al. A self-powered and flexible organometallic halide perovskite photodetector with very high detectivity [J]. Advanced Materials, 2018, 30(8): 1704611.
- [220] Zheng W, Lin R, Ran J, et al. Vacuum-ultraviolet photovoltaic detector[J]. ACS Nano, 2018, 12(1): 425-431.
- [221] Su L X, Yang W, Cai J, et al. Self-powered ultraviolet photodetectors driven by built-in electric field[J]. Small, 2017, 13(45): 1701687.
- [222] Wu Z P, Jiao L, Wang X L, et al. A self-powered deep-ultraviolet photodetector based on an epitaxial $\text{Ga}_2\text{O}_3/\text{Ga : ZnO}$ heterojunction [J]. Journal of Materials Chemistry C, 2017, 5(34): 8688-8693.
- [223] Zhao B, Wang F, Chen H Y, et al. An ultrahigh responsivity ($9.7 \text{ mA} \cdot \text{W}^{-1}$) self-powered solar-blind photodetector based on individual ZnO- Ga_2O_3 heterostructures [J]. Advanced Functional Materials, 2017, 27(17): 1700264.
- [224] Arora K, Goel N, Kumar M, et al. Ultrahigh performance of self-powered $\beta\text{-}\text{Ga}_2\text{O}_3$ thin film solar-blind photodetector grown on cost-effective Si substrate using high-temperature seed layer [J]. ACS Photonics, 2018, 5(6): 2391-2401.
- [225] Ye K, Liu L X, Liu Y J, et al. Lateral bilayer $\text{MoS}_2\text{-WS}_2$ heterostructure photodetectors with high responsivity and detectivity [J]. Advanced Optical Materials, 2019, 7(20): 1900815.
- [226] Chen H Y, Lu Y, Li C, et al. Multilayer PtSe₂/TiO₂ NRs Schottky junction for UV photodetector [J]. Acta Optica Sinica, 2020, 40(20): 2025001.
- 陈红云, 鲁玉, 李辰, 等. 多层 PtSe₂/TiO₂ 纳米棒肖特基结紫外光电探测器[J]. 光学学报, 2020, 40(20): 2025001.
- [227] He C R, Guo D Y, Chen K, et al. $\alpha\text{-}\text{Ga}_2\text{O}_3$ nanorod array- Cu_2O microsphere p-n junctions for self-powered spectrum-distinguishable photodetectors [J]. ACS Applied Nano Materials, 2019, 2(7): 4095-4103.
- [228] Mitra S, Pak Y, Xin B, et al. Solar-blind self-powered photodetector using solution-processed amorphous core-shell gallium oxide nanoparticles [J]. ACS Applied Materials & Interfaces, 2019, 11(42): 38921-38928.
- [229] Li S, Yan Z Y, Liu Z, et al. A self-powered solar-blind photodetector with large V_o enhancing

- performance based on the PEDOT: PSS/Ga₂O₃ organic-inorganic hybrid heterojunction [J]. Journal of Materials Chemistry C, 2020, 8(4): 1292-1300.
- [230] Wang Y F, Li L, Wang H B, et al. An ultrahigh responsivity self-powered solar-blind photodetector based on a centimeter-sized β -Ga₂O₃/polyaniline heterojunction [J]. Nanoscale, 2020, 12(3): 1406-1413.
- [231] Hawash Z, Ono L K, Qi Y B. Recent advances in spiro-MeOTAD hole transport material and its applications in organic-inorganic halide perovskite solar cells [J]. Advanced Materials Interfaces, 2018, 5(1): 1700623.
- [232] Wei J, Li H, Zhao Y C, et al. Suppressed hysteresis and improved stability in perovskite solar cells with conductive organic network [J]. Nano Energy, 2016, 26: 139-147.
- [233] Yan Z Y, Li S, Liu Z, et al. High sensitivity and fast response self-powered solar-blind ultraviolet photodetector with a β -Ga₂O₃/spiro-MeOTAD p-n heterojunction [J]. Journal of Materials Chemistry C, 2020, 8(13): 4502-4509.

Advances in Ga₂O₃-Based Solar-Blind Ultraviolet Photodetectors

Wang Jiang, Luo Linbao*

School of Electronic Science and Applied Physics, Hefei University of Technology, Hefei, Anhui 230009, China

Abstract

Significance The sunlight with a wavelength shorter than 280 nm cannot penetrate the atmosphere and reach the surface of the earth, for which the 200–280 nm waveband is typically referred to as solar-blind region. In recent years, solar-blind ultraviolet photodetectors are widely used in military and civil fields such as missile guidance, space secure communications, ozone hole detection, and flame monitoring due to the advantages of low background noise and high sensitivity.

In recent years, the studies of solar-blind ultraviolet photodetectors have mainly focused on wide-bandgap semiconductor materials such as Al_xGa_{1-x}N, Mg_xZn_{1-x}O, and Ga₂O₃. The bandgap of Al_xGa_{1-x}N and Mg_xZn_{1-x}O is located in the solar-blind region mainly by adjusting the relative composition of Al and Mg. Owning to the relatively high adhesion coefficient and low surface mobility of Al atoms, Al_xGa_{1-x}N with high Al content will lead to a larger dislocation density of the epitaxial layer, while phase segregation phenomena are often present for Mg_xZn_{1-x}O with high Mg contents. These factors will lead to poor device performance. Ga₂O₃ is a representative ultra-wide bandgap semiconductor material, with a typical band ranging from 4.2 to 5.3 eV that almost occupies the entire solar-blind region of the solar spectrum. The relatively large bandgap renders it as an ideal candidate for solar-blind ultraviolet detection application. Thanks to the rapid advances in materials synthesis technique, we has witnessed a significant progress in solar-blind ultraviolet photodetectors based on Ga₂O₃ in the past decade. By this token, it is necessary to summarize the recent advances, which may be beneficial for bringing out new high-performance devices with new geometries.

Progress In the past few years, various fabrication technologies have been widely adopted to synthesize Ga₂O₃ materials with different crystal structures. For example, in 2004, the β -Ga₂O₃ single crystals of 1 inch (1 inch = 2.54 cm) in diameter have been successfully grown by floating zone for the first time in Japan. Meanwhile, the domestic research on the growth of β -Ga₂O₃ single crystals has achieved remarkable results. In 2006, Shanghai Institute of Optics and Fine Mechanics employed the same floating zone to grow the β -Ga₂O₃ single crystal. Meanwhile, Tianjin Institute of Electronic Materials has achieved the growth of 2-inch β -Ga₂O₃ single crystals by using a new edge-defined film-fed growth method in 2018.

What is more, various solar-blind ultraviolet photodetectors composed of different forms of Ga₂O₃ with a variety of device geometries have been investigated. Some effective device optimization approaches such as controlled doping and light manipulation have been introduced to boost the photoresponse of the Ga₂O₃ based devices. For instance, Sooyeon et al. from Korea University fabricated the photodetector based on the back-gated field-effect transistor structure using exfoliated β -Ga₂O₃ flakes, whose maximum responsivity of the device exceeds 10⁴ A/W (Fig. 4). Tao's research group from Shandong University has fabricated the Ga₂O₃ field-effect-transistor-based solar-blind photodetector, its responsivity is up to 10⁵ A/W, and the external quantum efficiency exceeds 10⁶ %. Besides, our

group has reported a catalyst-free vapor-solid growth technique for synthesizing β -Ga₂O₃ nanowires with single-crystalline quality. The photodetector based on β -Ga₂O₃ nanowires can operate properly at a large applied bias of 200 V with the responsivity being enhanced to as high as 10³ A/W, and the external quantum efficiency can reach 10⁵ %. Fang's research group from Fudan University has fabricated a high-performance solar-blind avalanche photodetector based on highly crystallized ZnO-Ga₂O₃ core-shell heterojunction. The responsivity can reach up to 10³ A/W under -10 V bias, and the corresponding external quantum efficiency is as high as 10⁶ % [Figs. 13(b)–(d)]. Moreover, the solar-blind photodetectors based on Ga₂O₃ heterojunction, p-n junction, and Schottky junction with typical self-powered behavior can work normally without external power supply, which might find potential application in special environments.

Conclusions and Prospects In summary, we have witnessed extensive progress in Ga₂O₃ materials and solar-blind ultraviolet photodetectors in the past decade. In respect of material synthesis, the Ga₂O₃ single crystals can be grown at present, and the process route for depositing high-quality and large-area Ga₂O₃ thin films by MOCVD, MBE, magnetron sputtering, and other technologies is mature. Solar-blind photodetectors based on different forms of Ga₂O₃ have shown superior device performance including high responsivity and external quantum efficiency. What is more, the dark current of the device is as low as 1 pA, and the response speed is in the order of μ s. It is believed that the study of Ga₂O₃ device will mainly focus on the following aspects. First, We need accurately control the size and morphology of Ga₂O₃ nanomaterials and develop new approach such as doping to reduce the surface state and control internal defects, which is essential for the development of high-performance devices. Second, the effect of defects on crystal quality in single crystals growth, which is an important factor to grow high quality Ga₂O₃ single crystal, should be extensively studied. Third, the p-type conductivity of Ga₂O₃ material remains an unsolved problem, which severely limits its application in optoelectronics and power devices. Finally, relevant integration technologies should be developed to solve the problems of device arrangement and assembly. Large area array detectors are to be developed such as focal plane solar-blind imaging systems with the advantages of low power consumption, small size, good compatibility with CMOS readout circuits, and high integration. Additionally, the development of integrated circuit technology that is suitable for Ga₂O₃ related focal plane array is also very important. It is believed that through the continuous efforts in this field, the Ga₂O₃ based solar-blind ultraviolet photodetectors will be able to be applied to national defense military and civilian fields as soon as possible.

Key words photodetector; gallium oxide; ultra-wide bandgap semiconductor; solar-blind ultraviolet; photoresponse

OCIS codes 040.5160; 040.7190; 310.6845; 230.4000